690136

A Study of the Delivery Ratio Characteristics of Crankcase-Scavenged Two-Stroke Cycle Engines

Kazunari Komotori and Eiichi Watanabe
Keio University

ABSTRACT

In order to increase the air charge of crankcase-scavenged two-stroke cycle engines, the relations between delivery ratio and engine speed were investigated on a rotary disc-valve inlet port engine and on a conventional piston-valve inlet port engine by varying through wide limits the angle area and timing of the inlet port.

For the inlet port configuration tested on the first engine, it was found that there was an optimum cut angle of the rotary disc valve, which produced a certain angle area. To improve the delivery ratio characteristics at a given speed, it was not necessary to change this angle area; it was effective to change only the timing of the inlet port by shifting the disc valve around the crankshaft.

For the piston-valve inlet port engine, the results showed that a wide, low port, which was also found to have a higher flow coefficient, produced a higher delivery ratio over the entire engine speed range than a narrow, high port. For the configuration tested (with no inlet or exhaust pipes), the maximum delivery ratio of the wide, low port was nearly in proportion to the effective crankcase stroke.

PART 1

CASE OF ROTARY DISC-VALVE INLET PORT ENGINE

THE OUTPUT CHARACTERISTICS of two-stroke cycle engines are determined mainly by the charging efficiency which is a product of the delivery ratio and the trapping efficiency.. With the same scavenging system, there is little difference in trapping efficiency at a specified delivery ratio. (1)* Therefore, the output characteristics of crankcase-scavenged two-stroke cycle engines with the same scavenging system depend chiefly on the delivery ratio.

When these engines are used as prime movers of motor-scooters or automobiles, it is usually not required to have the tuning effects from the inlet and/or exhaust pipe systems because of their vehicle characteristics. Under these circumstances, the approximate delivery ratio characteristics are obtained by motoring the engines. (2-5) This was also confirmed by the authors' preliminary test described in the Appendix. Consequently, the following tests were carried out in the motoring mode. The authors used an engine having a rotary disc-valve inlet port, which was varied by changing the disc valves and their phase angles to the crankshaft. On the other hand, the scavenging and exhaust ports, which were designed to give the best trapping efficiency, were left unchanged from their original design.

*Numbers in parentheses designate References at end of Part 1.

EQUIPMENT USED AND TEST PROCEDURES

The general specifications of the engine and equipment used are shown in Table 1 and Fig. 1. In order to avoid the

tuning effects from the inlet and/or exhaust pipe systems on the delivery ratio characteristics, the inlet port was connected with receiver C by a short, large diameter duct as illustrated in Fig. 2. The exhaust port opened directly to the atmosphere.

The pressure in receiver C was always kept equal to that of the atmosphere by a Roots blower with control valves. The flow rate to the engine was measured by round nozzles (0.59 in. ϕ, 0.47 in. ϕ) (6) attached to the surface of receiver A. Some of the disc valves with cut angles of 50-180 deg are shown in Fig. 3.

In order to minimize the effects caused by the thickness of the disc valves, the edges of the valves and the inlet port located in the valve cover were finished as illustrated in Fig. 2. To assure the correct opening and closure of the ports, the diameter of the piston was machined over its total length equal to the piston skirt diameter. The angle area of the inlet port was varied in seven steps by different cut angles of the disc valves. The disc valves were fabricated in such a way as to permit shifting around the crankshaft (by slots cut in the collar and a pin used to fix the disc valve) as shown in Fig. 3. Each slot permitted a 22.5 crankangle deg shift to the disc valve. Table 2 shows the tested angle areas and the inlet port timing. Under these inlet port conditions, the relations between the delivery ratio and the engine speed were investigated.

At the same time, pressure indicator diagrams in the crankcase were recorded using a low-pressure pickup (Model PR/1, Shinko Electric Corp.). In orienting the crank angle of the indicator diagrams, a combination of mirror and photocell pickup were used. The distances between the pressure pickup and the scavenging or inlet ports were nearly the same, about 0.31 in. Assuming the sonic velocity in the crankcase was 1100 ft/sec, the travel time of the wave between them was in the order of 2.3×10^{-4} sec. The shift in the indicator diagrams corresponding to this travel time was about the width of the diagram's line even at the maximum speed (n = 6120 rpm) recorded. Therefore, the authors

Table 1 - General Specifications of Yamaha YG-1 Engine

Type	Air-cooled, single-cylinder, Schnürle-scavenged, two-stroke cycle gasoline engine
Cylinder Bore and Stroke	1.85 in. × 1.65 in.
Cylinder Volume	4.45 cu in. (73 cc)
Rated Output	6.5 hp/7000 rpm
Compression Ratio	6.8:1
Crankcase Compression Ratio	1.39:1
Scavenging Port	Opened 55 deg bbdc, closed 55 deg abdc, angle area of 45.5 deg-in.^{2}
Exhaust Port	Opened 74 deg bbdc, closed 74 deg abdc, angle area of 51.7 deg-in.^{2}
Reduced Angle Area of Scavenging and Exhaust Ports	31.8 deg. in^2
Inlet Port	Variable, shifting, and changing disc valves

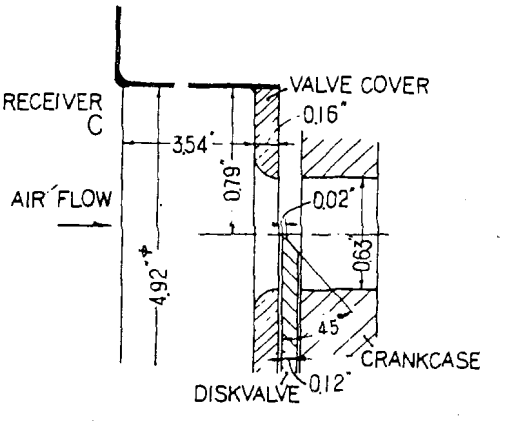

Fig. 2 - Inlet port in detail

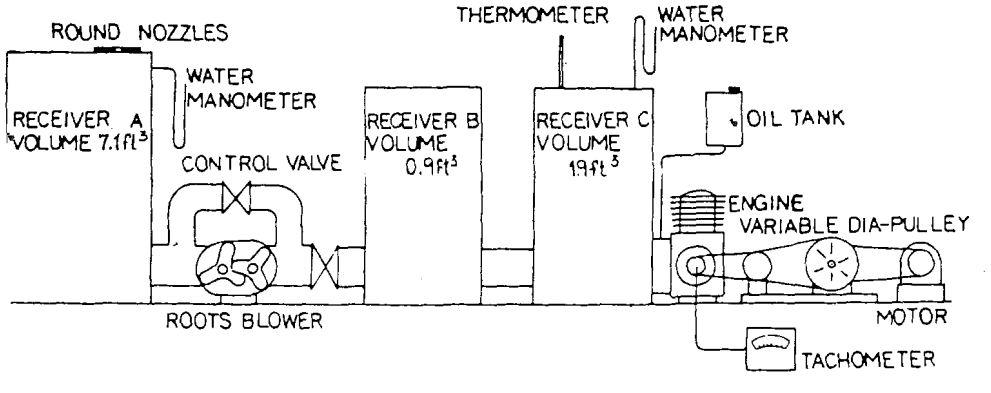

Fig. 1 - Test equipment used

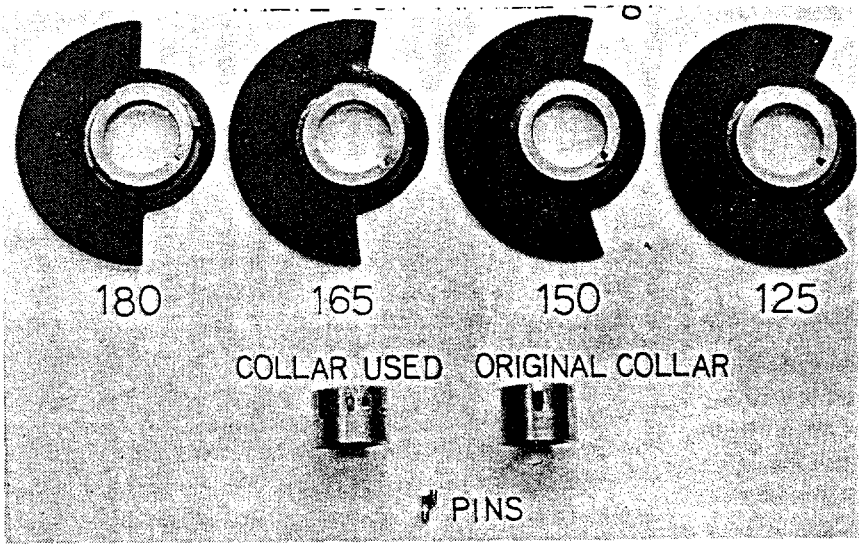

Fig. 3 - Disc valves having different cut-angles

Table 2 - Angle Areas and Inlet Port Timing

Valve Cut Angle, deg	Angle Area, deg-in.^{2}	Notation	Inlet Port Opens	Inlet Port Closes
50	21.3	50T1	92° 05' B. T.	11° 15' B. T.
		50T2	69° 35' B. T.	11° 15' A. T.
		50T3	47° 05' B. T.	33° 45' A. T.
		50T4	24° 35' B. T.	56° 15' A. T.
75	32.0	75T1	128° 20' B. T.	22° 30' B. T.
		75T2	105° 50' B. T.	0° 0'
		75T3	83° 20' B. T.	22° 30' A. T.
		75T4	60° 50' B. T.	45° 0' A. T.
100	42.5	100T1	142° 05' B. T.	11° 15' B. T.
		100T2	119° 35' B. T.	11° 15' A. T.
		100T3	97° 05' B. T.	33° 45' A. T.
		100T4	74° 35' B. T.	56° 15' A. T.
125	53.2	125T1	178° 20' B. T.	22° 30' B. T.
		125T2	155° 50' B. T.	0° 0'
		125T3	133° 20' B. T.	22° 30' A. T.
		125T4	110° 50' B. T.	45° 0' A. T.
		125T5	88° 20' B. T.	67° 30' A. T.
150	63.8	150T1	214° 35' B. T.	33° 45' B. T.
		150T2	192° 05' B. T.	11° 15' B. T.
		150T3	169° 35' B. T.	11° 15' A. T.
		150T4	147° 05' B. T.	33° 45' A. T.
165	70.2	165T1	196° 20' B. T.	0° 0'
		165T2	173° 50' B. T.	22° 30' A. T.
		165T3	151° 20' B. T.	45° 0' A. T.
		165T4	128° 50' B. T.	67° 30' A. T.
180	76.6	180T1	199° 35' B. T.	11° 15' A. T.
		180T2	177° 05' B. T.	33° 45' A. T.
		180T3	154° 35' B. T.	56° 15' A. T.
		180T4	131° 05' B. T.	79° 45' A. T.

B. T. = Before tdc
A. T. = After tdc

hink it is reasonable to represent the registered indicator liagrams as diagrams at the inlet or scavenging ports. This s also the case for the engine described in the Appendix.

DISCUSSION OF RESULTS

Figs. 4(a)-4(g) show delivery ratio curves as a function of engine speed. From these figures, it follows that there was certain engine speed, n_o, that produced the maximum delivery ratio, L_{max}. When the timing of the disc valve was shifted to give an earlier opening and closure of inlet port, the peak of the delivery ratio curve moved toward a lower engine speed. In Figs. 4(a)-4(d); the effects of changing the valve timing became less as the angle area of the inlet port decreased. On the other hand, when the angle area was large enough (Figs. 4(e)-4(g)), the effect of timing on n_o was remarkable and L_{max} became large.

Fig. 5 shows the superimposed envelopes corresponding to the delivery ratio curves of Figs. 4 A-G. These curves give the limiting delivery ratio curve of the engine when the angle area and timing of the inlet port were changed. Also, the nD values (n = engine speed in rpm, D = cylinder bore in in.) are indicated.

Fig. 6 shows the relation between L_{max} and K. K denotes the ratio of the inlet port angle area Fia and reduced (equivalent) angle area of the scavenging and exhaust ports Fra. Fig. 6 shows that there was an optimum inlet port angle area for a given Fra. As is shown in Fig. 5, the delivery ratio curve corresponding to the valve cut-angle of 165 deg (that is, Fia = 70.2 deg-in.^{2}, Fig. 4F) gives the largest delivery ratio over the entire engine speed range. That is, for the engine used, the optimum value of K was around 2.2. When Fia was larger or smaller than this value, the delivery ratio became smaller. From these figures it follows that to obtain a large delivery ratio for the engine over a wide speed range, it is unnecessary to vary Fia according to the change of engine speed; it is necessary only to shift the timing of the inlet port opening and closure using a disc valve with a certain cut-angle. Fig. 4F shows that the shift angle of the disc valve needed was around 22.5 crank angle deg, which corresponds to 9.6 deg-in.^{2} in angle area, as the shaded area Foa in Fig. 7 shows. Furthermore, when expressed in relation to the optimum inlet port angle area, Foa becomes about 14% of Fia.

ANALYSIS OF PRESSURE INDICATOR DIAGRAMS - In order to understand the phenomena better, crankcase indicator diagrams were recorded for the case of a disc valve with a cut-angle 165 deg, which showed the most favorable

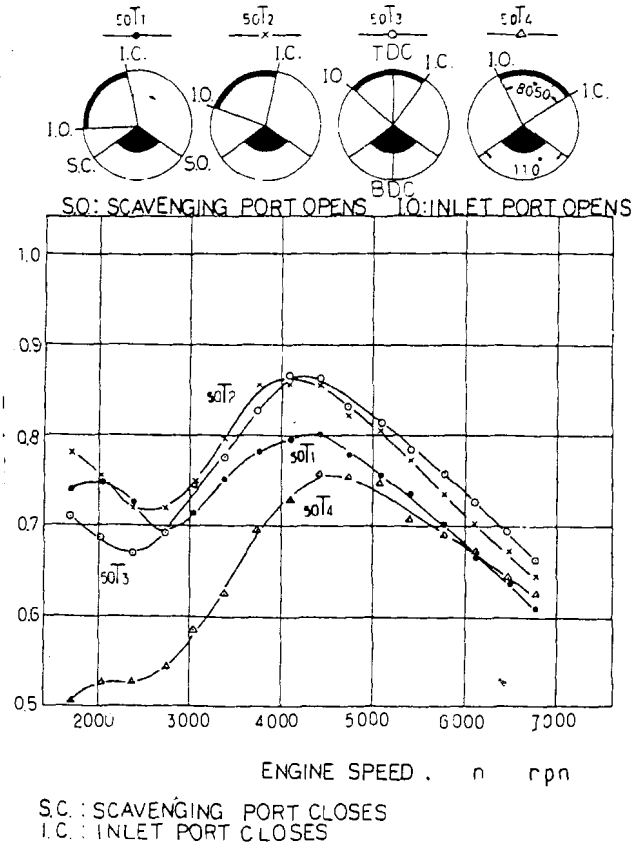

Fig. 4 (a) - Relation between delivery ratio and engine speed, 50 deg valve cut-angle

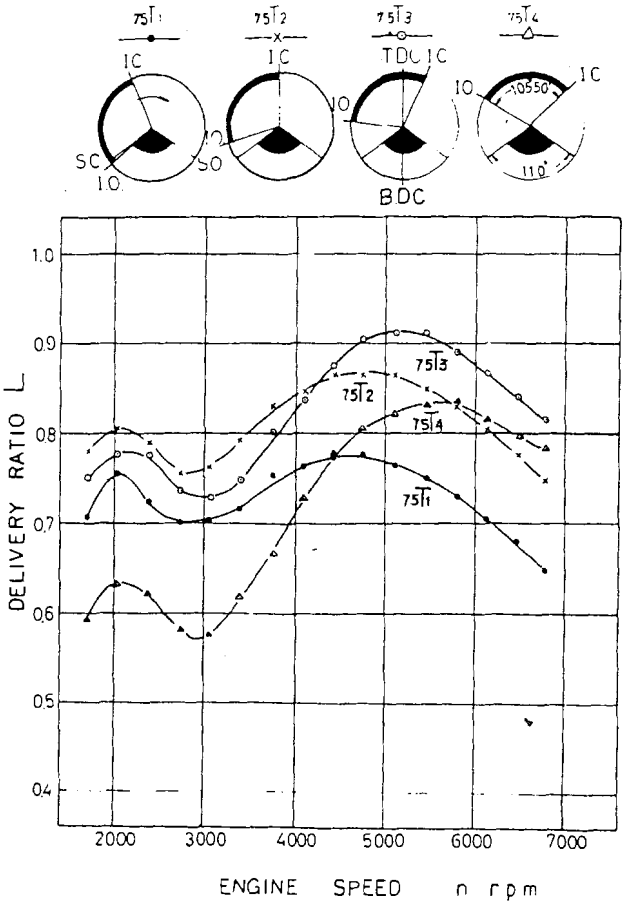

Fig. 4 (b) - Relation between delivery ratio and engine speed, 75 deg valve cut-angle

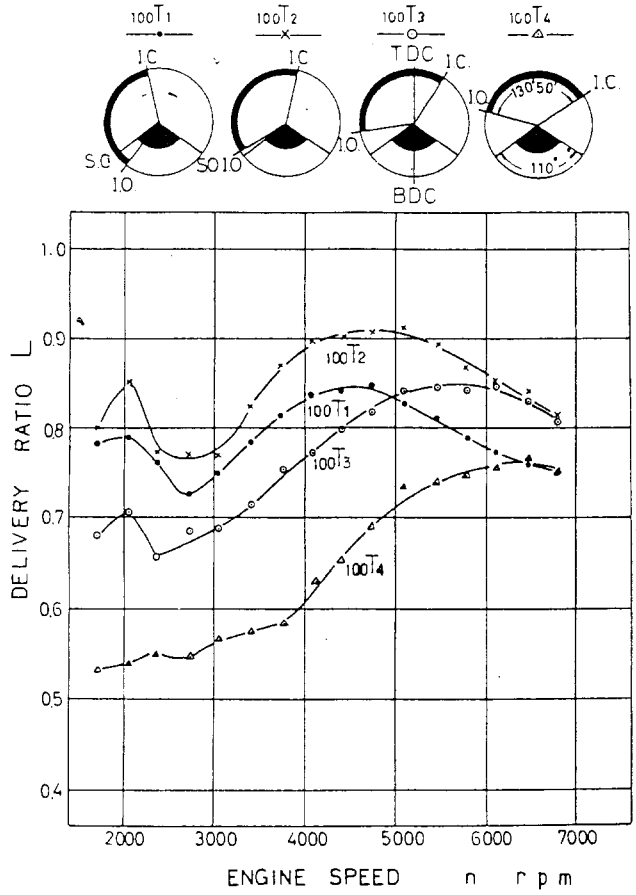

Fig. 4 (c) - Relation between delivery ratio and engine speed, 100 deg valve cut-angle

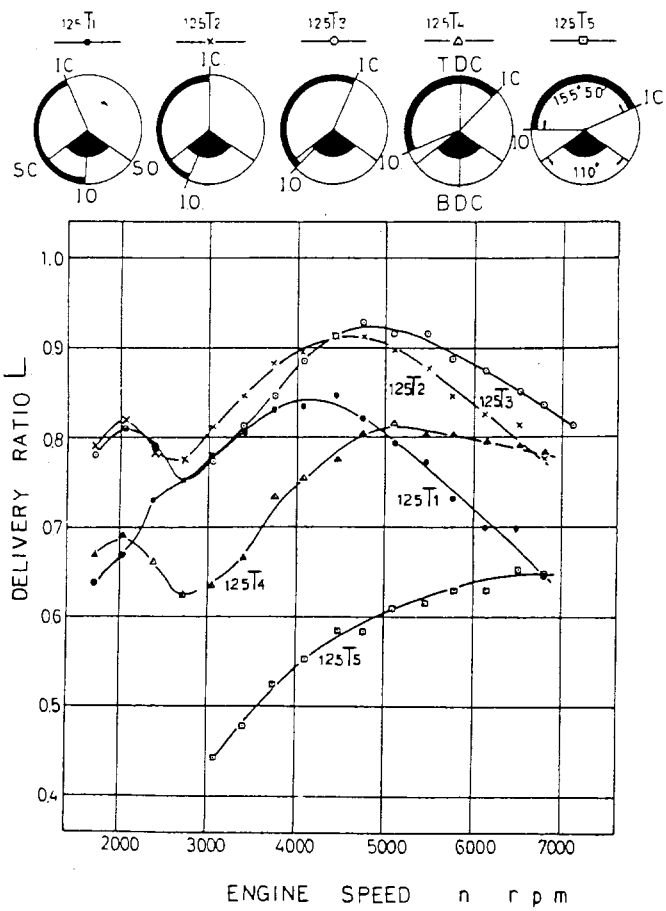

Fig. 4 (d) - Relation between delivery ratio and engine speed, 125 deg valve cut-angle

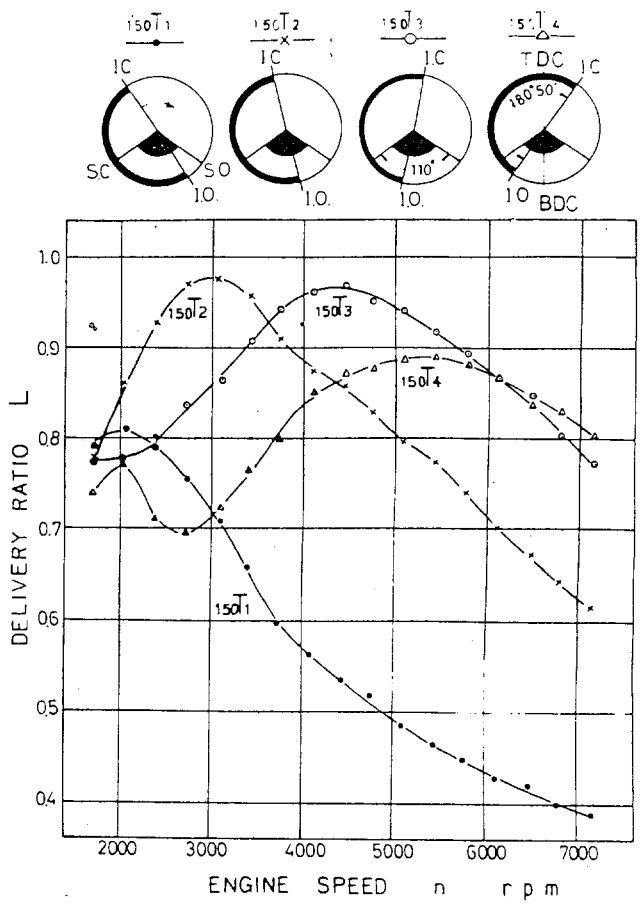

Fig. 4 (e) Relation between delivery ratio and engine speed, 150 deg valve cut-angle

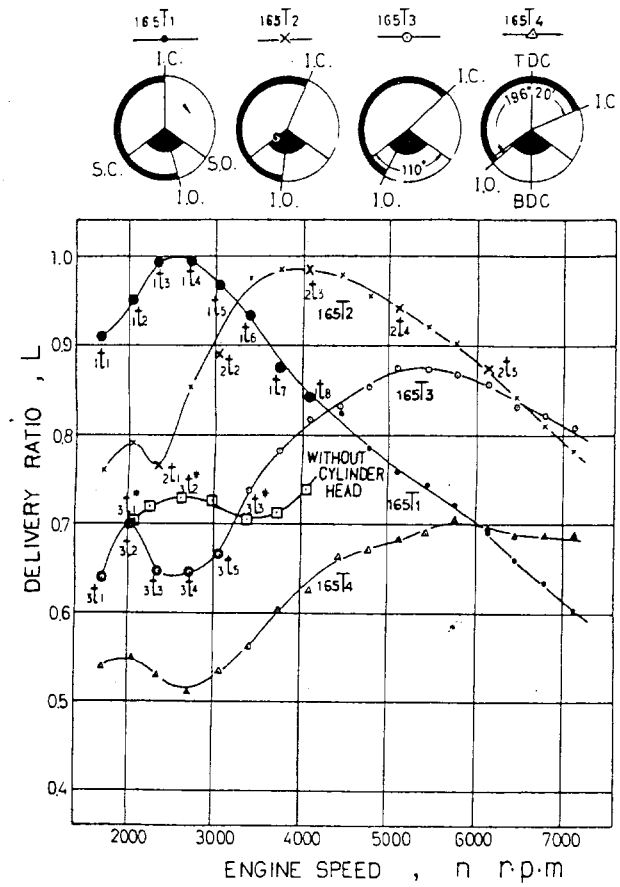

Fig. 4(f) Relation between delivery ratio and engine speed, 165 deg valve cut-angle. Notations $_{1}^{t}{}_{1\text{-}7}$, $_{2}^{t}{}_{1\text{-}5}$, $_{3}^{t}{}_{1\text{-}5}$, $_{3}^{t^{*}}{}_{1\text{-}3}$ correspond to each indicator diagram in Figs. 9, and 12-16

elivery ratio characteristics. Figs. 8(a)-(d) show the repre-ntative photographs of the indicator diagrams. Figs. 9 and -17 show the superimposed indicator diagrams in relation engine speed. The notation attached to each of the in-cator diagrams represents the measured points on the de-very ratio curves in Fig. 4(f).

GENERAL CHARACTERISTICS OF DELIVERY RATIO GAINST ENGINE SPEED - Fig. 9 shows the indicator dia-ams of $_{165}T_2$ which showed favorable delivery ratio alues over a relatively wide engine speed range.

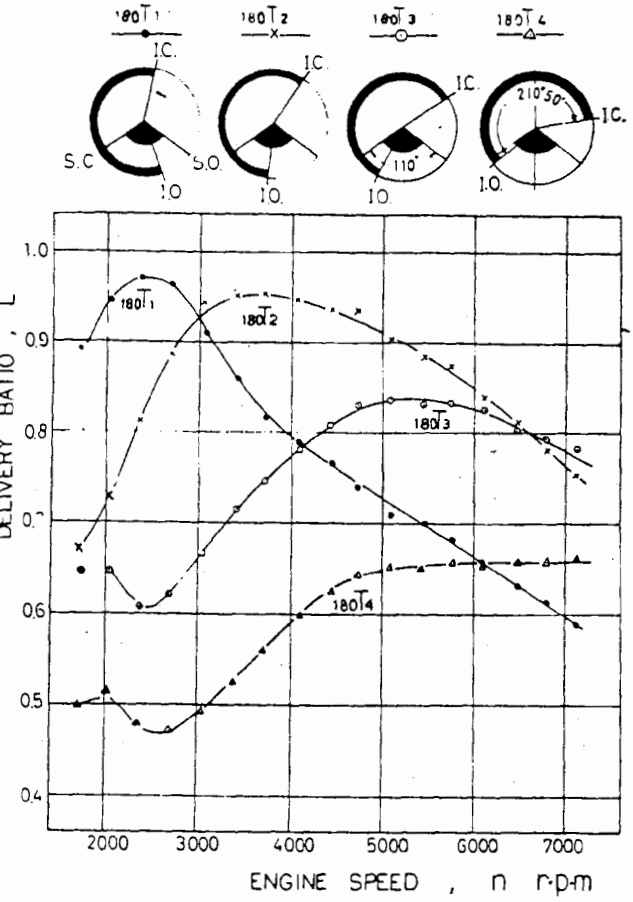

ig. 4 (g) - Relation between delivery ratio and engine peed, 180 deg valve cut-angle

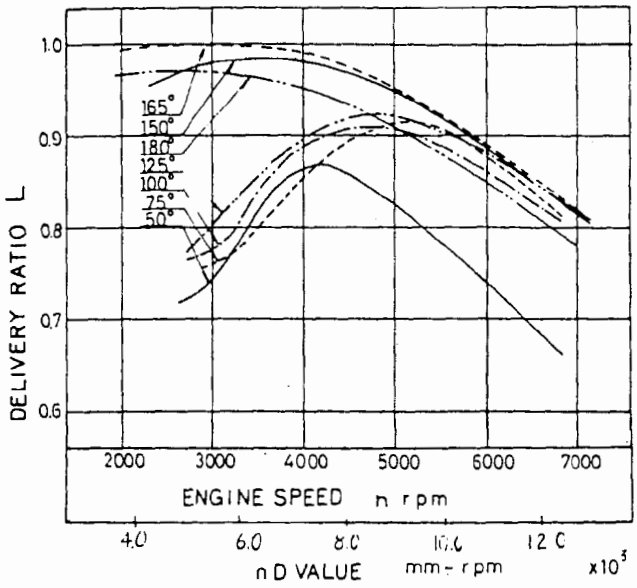

Fig. 5 - Relation between delivery ratio and engine speed. Envelopes from Figs. 4 a-g give limiting delivery ratio curve

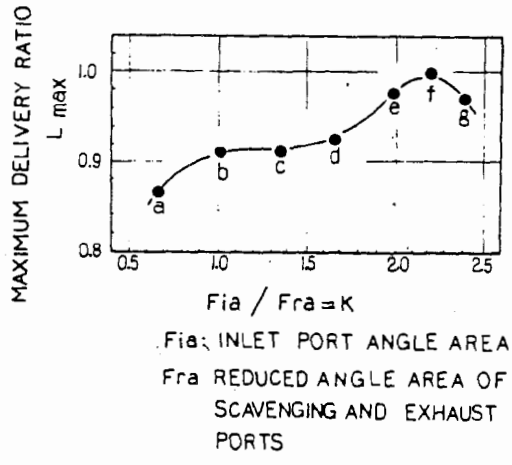

Fig. 6 - Relation between maximum delivery ratio and K. A-g correspond to the maximum delivery ratio in Fig. 4 (a) - 4 (g)

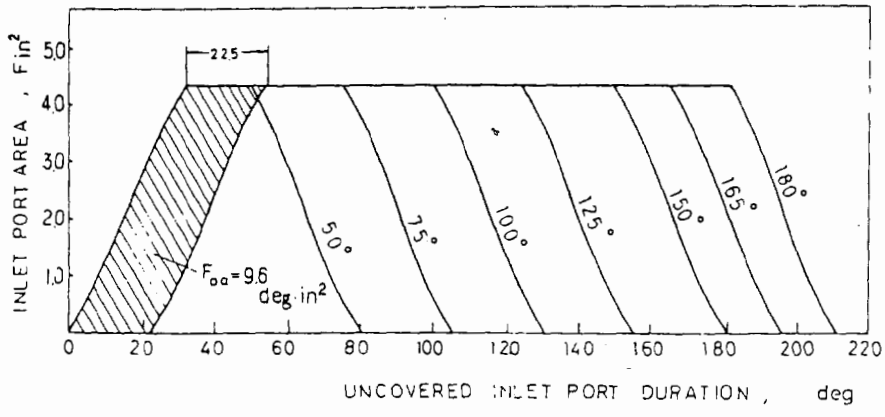

g. 7 - Relation between inlet port ea and uncovered inlet port duration. oa indicates change of inlet port angle ea corresponding to 22.5 crank angle g valve shift

At the lowest speed, $_2t_1$, the reduced angle area of the scavenging and exhaust ports Fra was too large, so the pressure in the crankcase P dropped to atmospheric long before scavenging port closure SC. An overexpansion period of P (that is, a "low tide," which is a negative pressure period usually observed in crankcase-scavenged two-stroke cycle engines) is seen right after inlet port opening IO. As the scavenging and exhaust ports of the engine used were nearly rectangular, the uncovered reduced port area Fr curve as a function of crank angle was convex, that is, $d^2Fr/d\theta^2 < 0$, at the beginning of port opening (Fig. 10). Therefore, the rate of increasing Fr was comparatively high. On the other hand, the inlet port had an oval shape and the uncovered port area Fi curve was concave, that is, $d^2Fi/d\theta^2 > 0$, at the beginning of port opening. Thus, the rate of increasing Fi was low. Therefore, an ineffective angle after IO occured. That is, although the inlet port was open during the "low tide" of P, the uncovered port area was not enough and the reverse flow from scavenging port was probably appreciable. As P at IC was almost atmospheric, the reverse flow from the inlet port during the tdc-IC period may also have been appreciable. Therefore, at this low speed, owing to the reverse flows from both the inlet and scavenging ports, the delivery ratio was small. The measured delivery ratio L = 0.77 corresponded to the value 1.30/1.65 = 0.79, where 1.30 in. was the effective crankcase stroke which corresponds to the SC-IO period and 1.65 in. was the piston stroke.

At a higher speed, $_2t_2$, P dropped below atmospheric after IO after a short delay. This time the inlet port was sufficiently open, thus the reverse flow from the scavenging port was probably less than in case of $_2t_1$; consequently, the delivery ratio was larger.

At $_2t_3$, the delivery ratio reached a maximum, L = 0.98. In this case, the lowest P during "low tide" ocurred at SC, while the inlet port was sufficiently open. On the other hand P became atmospheric at tdc, then rose during the tdc-IC period. Inasmuch as there was no sudden pressure difference before and after IC and there was a smooth increase of P, there was probably little reverse flow from the inlet port during the tdc-IC period. Although P was fairly high at IO, there existed an ineffective angle at the beginning of the inlet port opening as already stated, so this case may be stated as follows: There was no reverse flow from either the inlet or the scavenging ports, that is, the effective crankcase stroke nearly coincided with the piston stroke and the largest delivery ratio was obtained.

As the engine speed increased to $_2t_4$, $_2t_5$, Fra became inadequate and P remained above atmospheric even at SC. That is, the reverse flow from the inlet port at the beginning of port opening increased. As the angle area of the inlet port also became inadequate, P was below atmospheric at tdc and finally rose to atmospheric at IC. After $_2t_4$, both Fra and Fia became inadequate, and the delivery ratio became smaller.

The small fluctuations observed on the indicator diagrams at $_2t_5$ may have been caused by the relatively low natural frequency of the low pressure pickup.

WITH LARGE OVERLAP IN UNCOVERED PERIOD OF INLET AND SCAVENGING PORTS - Each of $_{150}T_2$, $_{165}T_1$, $_{180}T_1$ had a disc valve with a large cut-angle. In these cases, IO and IC came near bdc and tdc, respectively. This caused an overlap period between IO and SC where both the inlet and scavenging ports were open as illustrated (hatched area) in Figs. 10 and 11. With these overlap periods, the delivery ratio rose noticeably in the lower speed range, as indicated in Figs. 4(e)-(g). Fig. 12 shows the crankcase

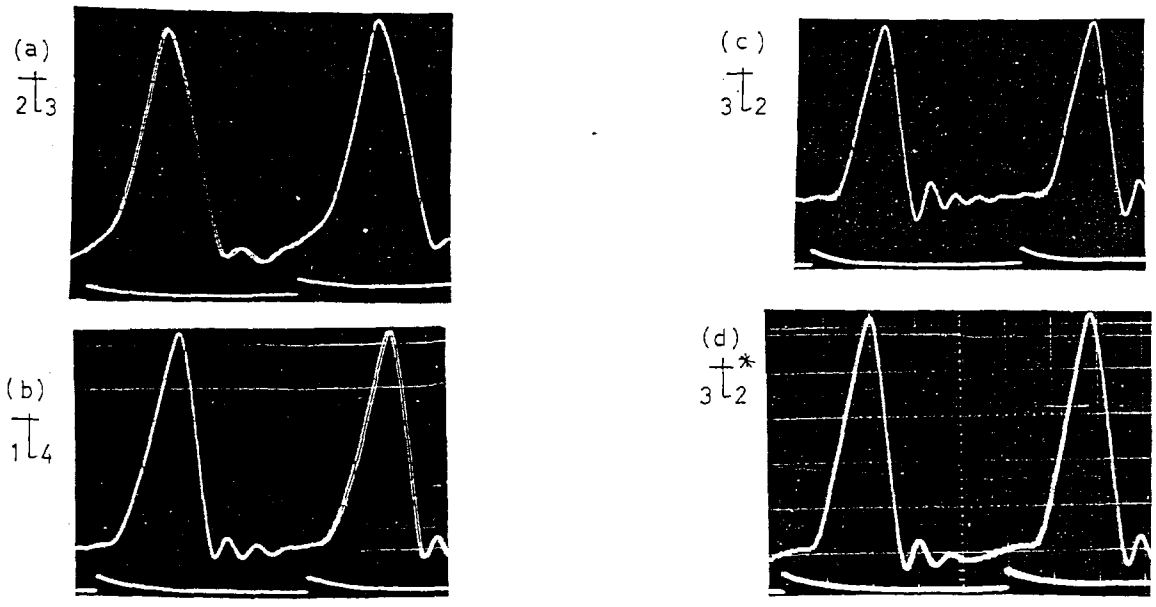

Fig. 8 - Representative photographs of the crankcase indicator diagrams for rotary disc-valve inlet port engine

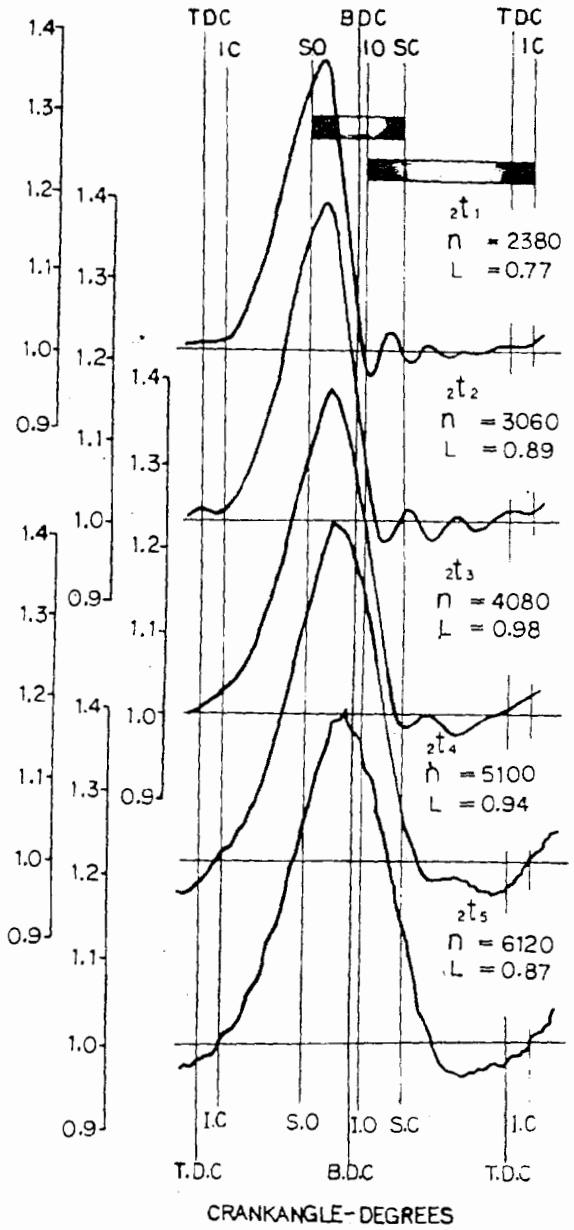

g. 9 - Crankcase indicator diagrams, case of $_{165}T_2$

indicator diagrams corresponding to $_{165}T_1$ in which this event is most remarkable.

At the lowest speed, $_1t_1$, Fra was too large, so P dropped to atmospheric even before bdc. Between the bdc-SC period there should have been a reverse flow from the scavenging port. Although in this period the inlet port was sufficiently open, the reverse flow may not have been remarkable. IC coincided with tdc in this case, that is, there was no reverse flow from the inlet port around tdc. Regarding the effective crankcase stroke as (bdc-SC period)/2 + (SC-tdc period) which corresponded to 1.52 in., the measured delivery ratio L = 0.91 nearly coincided with 1.52/1.65 = 0.92, where 1.65 in. was the piston stroke. Assuming that the mean P was about atmospheric during the bdc-SC period, the reverse flow from the scavenging port in the IO ~ SC period may be evaluated as about the same as that from the inlet port.

As the speed increased a little to $_1t_2$, P after SO dropped a little slower. Inasmuch as the uncovered inlet port area

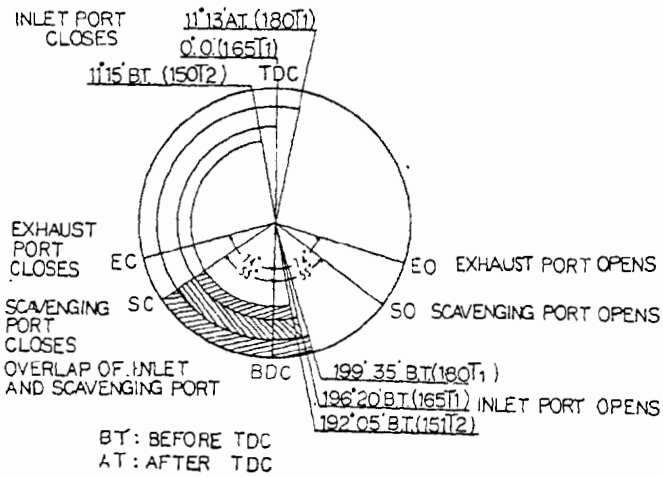

Fig. 11 - Port timing diagram

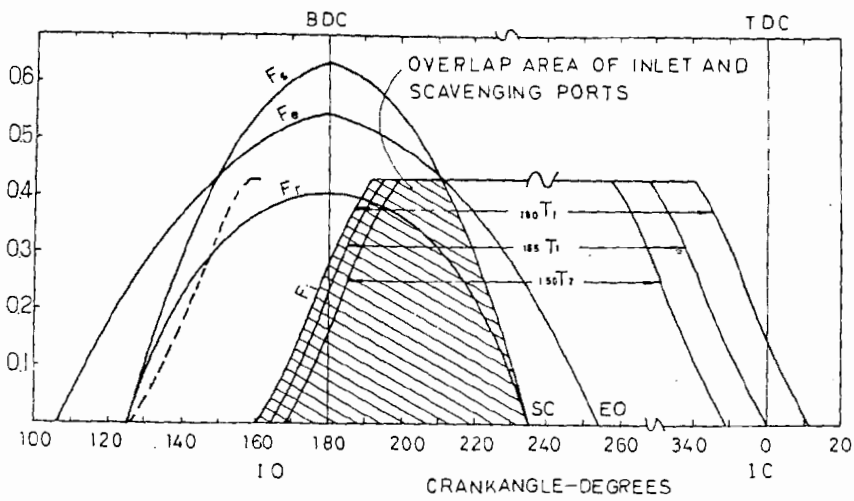

Fig. 10 - Relation between uncovered port area and crank angle

Fe : EXHAUST PORT AREA
Fr : REDUCED AREA OF EXHAUST
Fi : INLET PORT AREA
Fs : SCAVENGING PORT AREA
AND SCAVENGING PORT

in the "low tide" of P was larger than in the case of $_1t_1$, the reverse flow from scavenging port was less.

At $_1t_3$, $_1t_4$, the delivery ratio reached its maximum, L = 0.99. As P was about atmospheric at tdc (IC) in this case, the event may be stated as follows: The inlet port was sufficiently open in the "low tide" of P, which was very helpful in drawing fresh air into the crankcase. On the other hand, the scavenging port closed just before reverse flow occurred because of the inertia of the gases in the scavenging passages. (8) The effect was as if the effective crankcase stroke nearly coincided with the piston stroke and thus made the delivery ratio almost unity.

With further increases in engine speed $_1t_5$ - $_1t_8$, P dropped more slowly after SO, thus a higher P occurred at IO which made the reverse flow from the inlet port increase at the beginning of port opening. Thus, the delivery ratio values decreased.

WHEN DISC VALVE IS SHIFTED AROUND CRANKSHAFT - Figs. 13 and 14 show the crankcase indicator diagrams at the same engine speed but with the disc valve having the same cut angle shifted around the crankshaft.

In Fig. 13, although $_1t_3$, $_2t_1$, $_3t_3$ had the same uncovered inlet port duration, each of them had a 22.5 crankangle deg difference in timing. P_{max} was about the same and

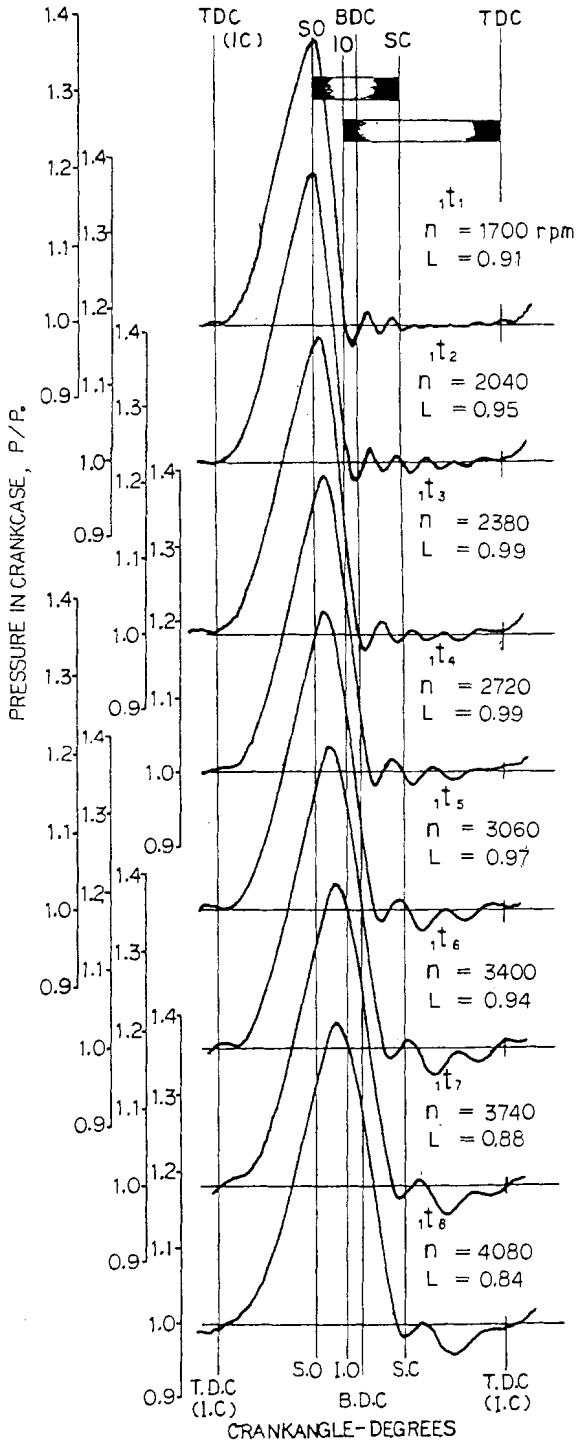

Fig. 12 - Crankcase indicator diagrams, case of $_{165}T_1$

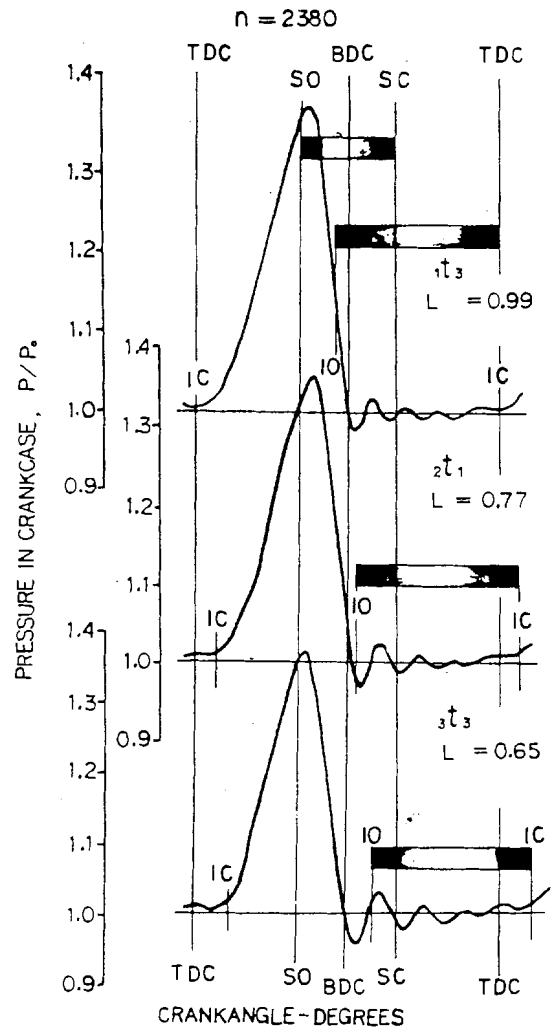

Fig. 13 - Crankcase indicator diagrams, cases of $_{165}T_1$, $_{165}T_2$ and $_{165}T_3$

there were few differences between them in the P curves after SO.

At $_1t_3$, as already stated, both IO and IC satisfied the optimum condition which produces the largest delivery ratio. At $_2t_1$, as explained, both IO and IC were too late to check the reverse flow from the scavenging and/or inlet ports. At $_3t_3$, as both IO and IC occurred much later, the reverse flow from both ports may have been appreciable and delivery ratio became smaller.

In Fig. 14, as the engine speed was higher than in Fig. 13, P dropped slowly after SO. At $_2t_3$, as already stated, both IO and IC satisfied the optimum condition which allows the minimum reverse flow. At $_1t_8$, IO was so early that the inlet port opened long before P dropped to atmospheric. Also, IC was too early for P to recover even atmospheric pressure. Therefore, the reverse flow from both the inlet and scavenging ports must have been appreciable.

From these figures it follows that there is an optimum shifting angle of the disc valve for a given engine speed.

LITTLE HILL ON DELIVERY RATIO CURVE IN LOW ENGINE SPEED RANGE - Little hills are observed on the delivery ratio curves in the low engine speed range, as indicated by each curve in Fig. 4. These hills are not as pronounced as the usual peaks of the delivery ratio curves. But this event occurred not only with the engine which had a rotary disc valve inlet port, but also with the engine having a piston-valve inlet port, as described in the Appendix. Furthermore, these hills are observed also in the literature. (9-11) This phenomenon, peculiar only to crankcase-scavenged two-stroke cycle engines, has never been discussed.

CASE OF ROTARY-VALVE INLET PORT ENGINE - Fig. 15 shows the representative crankcase indicator diagrams for $_{165}t_3$, whose delivery ratio curve is shown in Fig. 4(f). As the engine speed was relatively low, P dropped quickly to atmospheric after SO, then went into a "low tide." This negative pressure pulse generated pressure fluctuations in the crankcase, which were almost completely damped out at the end of the suction stroke. In view of the fact that these hills have almost no relation with the angle area and timing of the inlet port, as indicated in each curve of Fig. 4, attention is directed to P at SC.

At $_3t_1$, SC coincided with the second peak of P after SO. That is, the air flow into the crankcase decreased in the next cycle; thus, the delivery ratio was smaller. At $_3t_2$, as the engine speed increased, the entire pressure pulsation shifted to the right in the figure; therefore, SC oc-

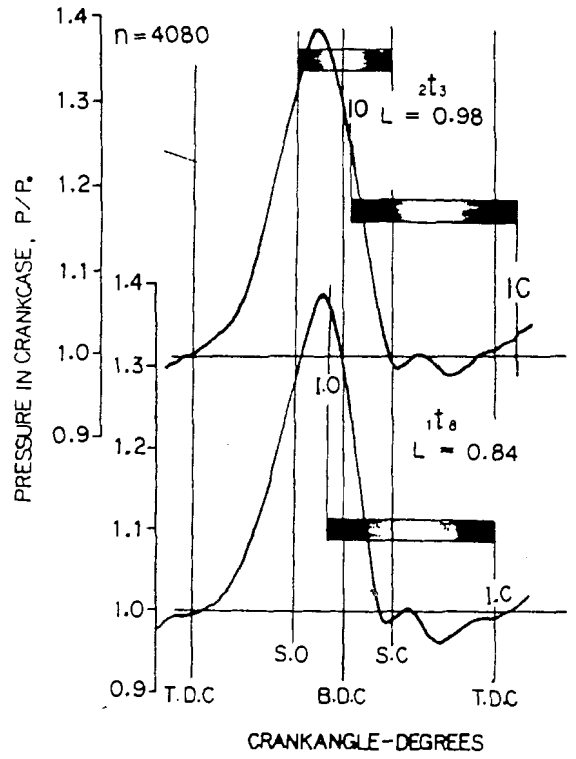

Fig. 14 - Crankcase indicator diagrams, cases of $_{165}T_2$ and $_{165}T_1$

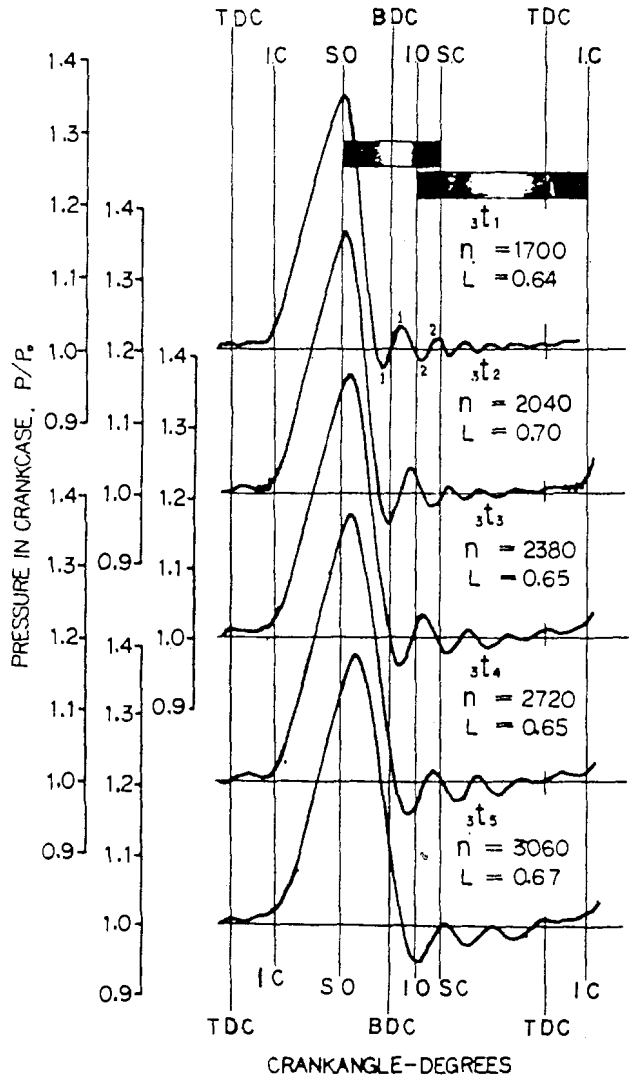

Fig. 15 - Crankcase indicator diagrams, case of $_{165}T_3$

curred during the second "low tide" of P. At $_3t_3$, the pressure pulsation shifted more and P was nearly atmospheric at SC. On the other hand, P at IC was about the same as at $_3t_1$, $_3t_2$, and $_3t_3$. Therefore, a little hill occurred on the delivery ratio curve before and after $_3t_2$. With a further increase in speed, $_3t_4$, besides the pressure pulsation being shifted more, the entire pressure wave dropped downward owing to the effect of the suction stroke. After $_3t_5$, as SC occurred during the first "low tide," the delivery ratio increased.

When the cylinder head was removed, Fra reached a maximum and coincided with the angle area of the scavenging port Fsa. In this case, P dropped more rapidly after SO and made it possible to reproduce the same event over a wider engine speed range, as illustrated by the dash line in Fig. 4(f). This is favorable for better analysis.

Fig. 16 shows the indicator diagrams of $_{165}T_3$ without the cylinder head. Notation $_3t_1^*$, $_3t_3^*$ correspond to the troughs before and after the hill. $_3t_2^*$ corresponds to the peak. SC coincided with the second peak of "high tide" at $_3t_1^*$, with the second peak of "low tide" at $_3t_2^*$, and with the first peak of "high tide" at $_3t_3^*$, respectively. From this, the event described above is better understood.

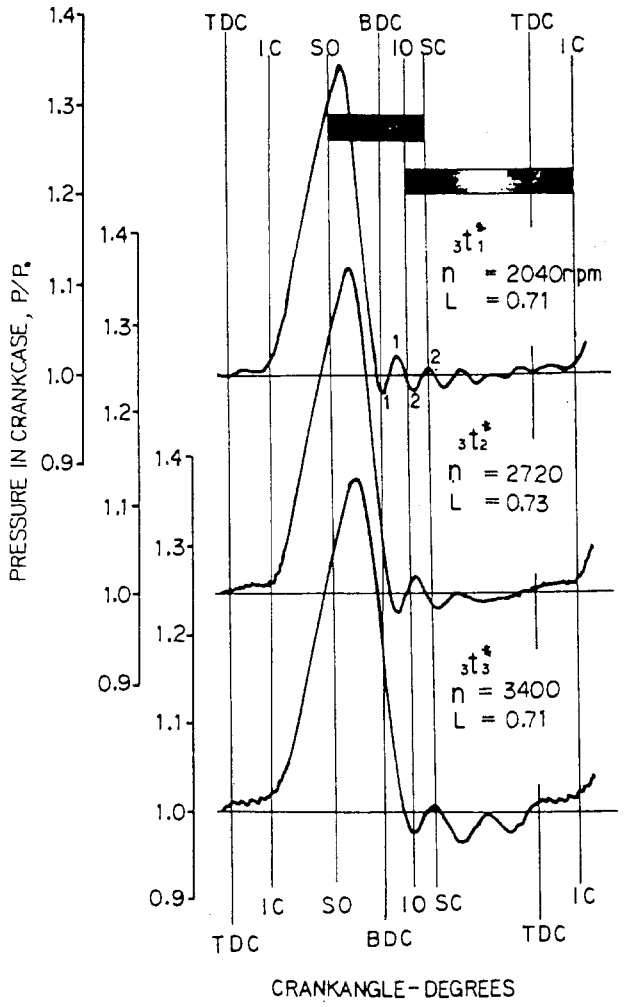

Fig. 16 - Crankcase indicator diagrams, case of $_{165}T_3$ (without cylinder head)

The natural frequencies of these pressure pulsations measured from the indicator diagrams were between 340-360 cps. There was no difference in these values with or without the cylinder head. Therefore, putting the cylinder volume aside, the crankcase volume and scavenging passages are noticed. Regarding the crankcase volume as V, the sonic velocity in the crankcase as C, the scavenging passages as a pipe having a cross-sectional area A and a length L, the natural frequency of the air in the crankcase f_c is expressed as $f_c = \frac{C}{2\pi}\sqrt{\frac{A}{VL}}$ (12). Using the measured values $A = 0.62$ in.^{2}, $L = 0.196$ in., $V = 11.8$ in.^{3} (this corresponded to the crankcase volume when the piston was located halfway between bdc and SC), and assuming $C = 1100$ ft/sec, then $f_c = 350$ cps, which coincided with the value from the indicator diagrams fairly well.

CASE OF PISTON-VALVE INLET PORT ENGINE - Fig. 17 shows the crankcase indicator diagrams of the engine with a piston-valve inlet port, whose general specifications are shown in Table A-1. Although in this case the air delivery was measured on the running (firing) engine, the blowdown angle area was adequate in the entire speed range and thus no abnormal pressure rise right after SO is observed. This reveals that there was no reverse flow into the crankcase. Because of this, the delivery ratio curve very nearly coincided with that obtained when motoring. (See Fig. A-3.)

In Fig. 17, P expanded below atmospheric after SO. This depression (negative pressure pulse) generated a little pressure fluctuation in the crankcase as in the case of the engine with a rotary disc valve inlet port. Since the inlet port was not open until after SC, this little pressure pulsation disappeared with decreasing P. On the other hand, right after IO, P recovered rapidly and went above atmospheric. This positive pressure pulse also generated a little pressure fluctuation in the crankcase, as observed around bdc.

First, attention is directed to P at SC. At SC, a lower P is more favorable for increasing the delivery ratio. At t_1, SC coincided with the second peak of "high tide" after SO. At t_2 and t_3, SC occurred during the second "low tide" of P. As the engine speed increased to t_4 and t_5, the whole pressure pulsation gradually shifted to the right. At t_6, SC nearly coincided with the first peak of "high tide."

Second, attention is directed to P at IC, where higher P is more favorable. At t_1, IC coincided with the second peak of "high tide." As the engine speed increased, t_2 - t_5,

the whole pressure pulsation gradually shifted to the right. At t_6, IC coincided with the first peak of "low tide."

When the pressure difference between IC and SC which governs the delivery ratio is considered in each case, it follows that a little hill on the delivery ratio curve will occur before and after t_2.

With further increase in the engine speed, SC comes into the first "low tide" and IC comes into the first "high tide" of P. When SC coincides with the first peak of "low tide" and IC with the first peak of "high tide," respectively, the maximum delivery ratio is obtained.

WHEN REDUCED AREA OF SCAVENGING AND EXHAUST PORTS IS CHANGED - In the test so far, the scavenging and exhaust ports were left unchanged. That is, the reduced angle area of the scavenging and exhaust ports Fra was kept constant. To investigate result with another Fra most simply the cylinder head was removed. This case corresponds to that in which the blowdown angle area is greatly increased; then Fra coincides with the angle area of the scavenging ports Fsa. One example of these cases is shown as dashed lines in Fig. 18. Solid lines represent the delivery ratio curves with the cylinder head. The speed n_o, which affects L_{max}, shifts widely to a higher engine speed, and L_{max} becomes larger. In view of the fact that even by increasing Fia, the delivery ratio curve doesn't exceed the limit curve (as illustrated in Fig. 5) it follows that the reason the delivery ratio is limited at the higher speeds is the shortage of Fra.

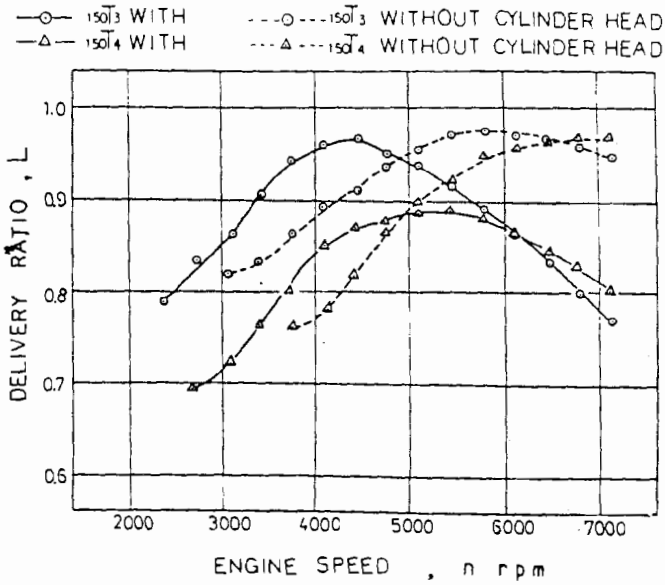

Fig. 18 - Relation between delivery ratio and engine speed, 150 deg valve cut-angle. Comparison of delivery ratio curves with and without cylinder head

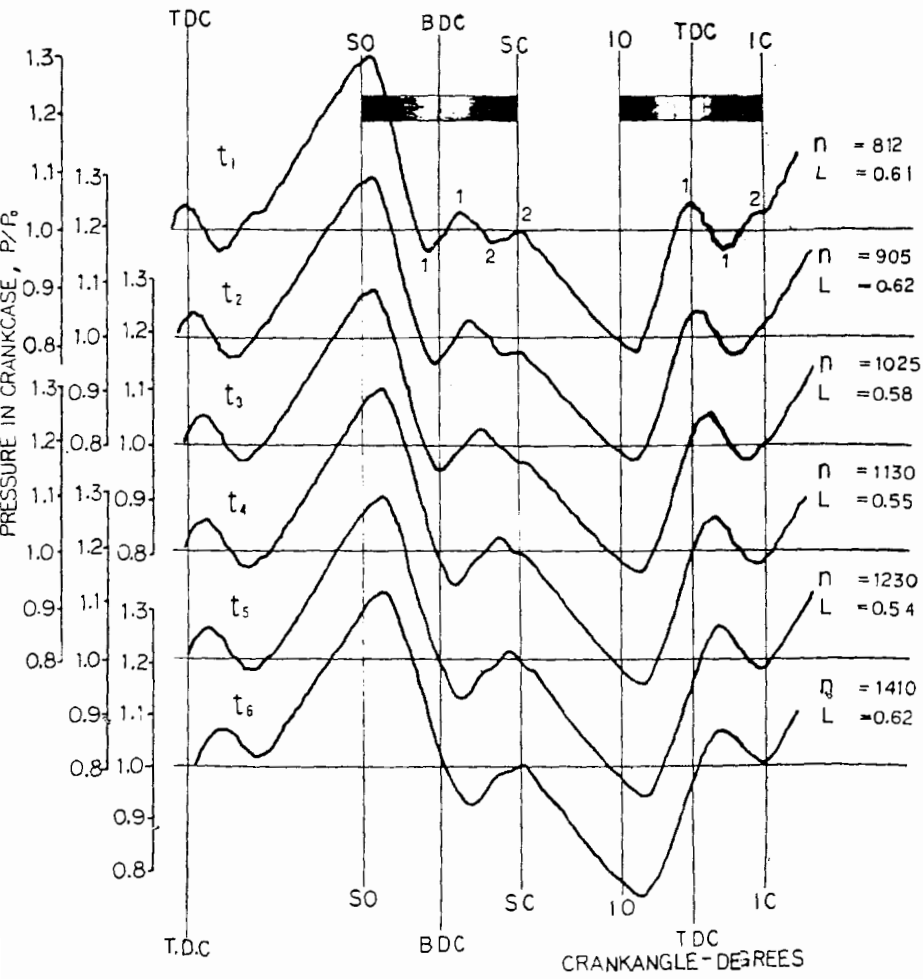

Fig. 17 - Crankcase indicator diagrams, case of the piston-valve inlet port engine described in Appendix A

On the other hand, in the low speed range, the delivery ratio curves with the cylinder head exceed those without the cylinder head. This may be explained as follows: Without the cylinder head, Fra (Fsa) is so large for the speed that P drops more rapidly than in case with the cylinder head. Therefore, reverse flow from the scavenging ports during the bdc-SC period increases.

In general, as it shortens the effective piston stroke, it is not easy to increase Fra. Therefore, it may be necessary to utilize the effects from the inlet and/or exhaust pipe systems to increase the delivery ratio in the high speed range.

CONCLUSIONS

By means of motoring a rotary disc valve inlet port engine having no tuning effects from the inlet and/or exhaust pipe systems, and by greatly changing the angle area and timing of the inlet port, the relations between delivery ratio and engine speed were investigated. At the same time, the pressure indicator diagrams in the crankcase were recorded. The results obtained are:

1. By changing the timing of the inlet port with a given angle area, the engine speed n_o, which produces the maximum delivery ratio, varies. Earlier opening and earlier closing of the inlet port makes n_o shift to a lower engine speed range.

2. To improve the delivery ratio characteristics, it is not necessary to change the angle area; it is effective to change only the timing of the inlet port by shifting the disc valve with an optimum cut angle around the crankshaft in accordance with the change of engine speed.

For the engine used, the value of (inlet port angle area)/(reduced angle area of the scavenging and exhaust ports) = 2.2, and a shifting angle of the disc valve around 20 deg, which corresponds to 14% of the inlet port angle area, produced the optimum results.

3. Proper overlap in the uncovered port period of the scavenging and inlet ports causes a noticeably large delivery ratio in the lower engine speed range.

4. Little hills observed on the delivery ratio curves of both engines with rotary disc valve and piston-valve inlet ports are peculiar only to crankcase-scavenged two-stroke cycle engines. When the scavenging port closure coincides with the peak of "low tide" and/or inlet port closure coincides with the peak of "high tide" of pressure pulsation in the crankcase, this event occurs.

5. As the reduced angle area of the scavenging and exhaust ports is small, it is useless to change the angle area and/or timing of the inlet port to increase the delivery ratio in the higher engine speed range.

ACKNOWLEDGMENTS

The authors wish to thank K. Kawashima at Yamaha Engine Corp. and Y. Yamaki at Fuji Heavy Industry Corp. who assisted with much of the experimental and construction work. S. Takeshita, K. Yamamoto, T. Okamura, M. Muto, T. Nakata, K. Miyake, and T. Koda were most closely associated with this work and their help is most sincerely appreciated.

The authors also wish to thank Dr. I. Watanabe and Dr. Benjamin L. Sheaffer for their appropriate guidance and advice.

SYMBOLS

Fi, Fs, Fe	= Area of inlet, scavenging, and exhaust ports, respectively
Fia, Fsa, Fea	= Angle-area of the inlet, scavenging, and exhaust ports, respectively
Fr, Fra	= Areas and angle areas of reduced port for scavenging and exhaust ports
L	= Delivery ratio
n	= Engine speed, rpm
P	= Pressure in crankcase
Po	= Ambient pressure
θ	= Crank angle, deg

REFERENCES, PART 1

1. H. List, "Der Ladungswechsel der Verbrennungskraftmaschine." Springer Verlag, Vol. 4 (1950), No. 2, p. 45.

2. T. Asanuma and N. Sawa, "On the Effects of Intake Pipe System in a Small Two-Stroke Cycle Gasoline Engine." Transactions, Japan Soc. Mech. Engrs., Vol. 25 (1959), No. 156, p. 834.

3. F. Nagao, U. Shimamoto, and M. Miyake, "Effect of the Induction Pipe in a Crankcase-Scavenged Two-Cycle Engine." Transactions, Japan Soc. Mech. Engrs., Vol. 26 (1961), No. 171, p. 1675. See also paper 670030, "The Effect of Crankcase Volume and the Inlet System on the Delivery Ratio of Two-Stroke Cycle Engines." Presented at SAE Automotive Engineering Congress, Detroit, January 1967.

4. S. Ishigami, "On Scavenging of the Crankcase Compression Type Two-Stroke Cycle Diesel Engine." Technical Reviews, Kagoshima University, Vol. 2 (1962), p. 23.

5. P. H. Schweitzer, "Scavenging of Two-Stroke Cycle Diesel Engines." New York: MacMillian, 1949, p. 192.

6. M. Maekawa, "On the Nozzles at Low Reynolds Numbers with a View of Measuring Pulsating Flow of Gases." Transactions, Japan Soc. Mech. Engrs., Vol. 37 (1934), No. 209, p. 599.

7. Ref. 4, p. 55.

8. W. Wilhelm, "Einfluss der Spulkanalabmessungen auf den Ladungswechsel kurbelkastengespulter Zweitakt-Motoren." Forsch. Landes. Nordrhein-Westfalen, No. 989, 1961.

9. F. Nagao, U. Shimamoto, H. Obayashi, and T. Kura "Effect of Crankcase Volume on the Delivery Ratio of a Crankcase-Scavenged Two-Cycle Engine." Transactions, Japan Soc. Mech. Engrs., Vol. 25 (1960), No. 152, p. 314.

See also SAE paper 670030, listed in Ref. 3.

10. E. Watanabe and K. Komotori, "Study of the Delivery Ratio Characteristics of a Crankcase-Scavenged Piston-Valve Inlet Port Two-Stroke Cycle Engine." Paper 156 presented at Meeting of Japan Soc. Mech. Engrs., 1966, p. 39.

11. Report of Lecture Meeting, Journals, Japan Soc. Mech. Engrs., Vol. 67 (1965), No. 545, p. 917.

12. E. Fiala and H. P. Willmeit, "Schwingungen in Gaswechselleitungen von Kolbenmaschinen." MTZ, Vol. 28 (1967), No. 4, p. 144.

APPENDIX A - Part 1

In the preliminary test, the delivery ratio curves of the motored and running (firing) engine were compared. To avoid the tuning effects from the carburetor or throttle in the intake system on the delivery ratio, a single-cylinder crankcase-scavenged two-stroke cycle diesel engine was used. The general specifications and test equipment used are shown in Table A-1 and Fig. A-1. To avoid the tuning effects from the inlet and/or exhaust pipe systems, both ports were connected to receivers through short ducts with large cross-sectional areas as shown in Fig. A-2. Fig. A-3 shows that there was almost no difference in the delivery ratio characteristics between the motored and running engines.

The brake mean effective pressure of Pme = 56.9 psi corresponds to 110% load for the engine.

Table A-1 - General Specifications of Robin DC 32 Engine, Huji Heavy Industry Corp.

Type	Air-cooled, single-cylinder, Schnürle-scavenged two-stroke cycle diesel engine
Cylinder bore × stroke	3.34 in. × 3.39 in.
Cylinder volume	34.6 cu in. (567 cc)
Rated output	10 hp/2000 rpm
Compression ratio	23:1
Crankcase compression ratio	1.35:1
Inlet port	Opened 52 deg btdc, closed 52 deg atdc
Scavenging port	Opened 56 deg bbdc, closed 56 deg abdc
Exhaust port	Opened 71 deg bbdc, closed 71 deg abdc

1 : OIL TANK, FUELTANK
2 : OIL METERING DEVICE
3 : FUEL METERING DEVICE
4 : WATER MANOMETER
5 : WATER MANOMETER
6 : THERMOMETER
7 : CYLINDERHEAD, EXHAUST GAS TEMP. mV METER
8 : FILTER TYPE SMOKE METER
9 : THERMO COUPLE
10 : CONTROL VALVE
11 : RUBBER MEMBRANCE
12 : ROUND NOZZLES
13 : ROOTS BLOWER
14 : RUBBER MEMBRANCE
15 : RECEIVER B (7.1ft³)
16 : ENGINE
17 : RECEIVER C (7.1ft³)
18 : OUT DOORS
19 : OVER FLOW
20 : WATER SUPPLY
21 : WATER HEAD TANK
22 : TACHOMETER
23 : WATER DYNAMOMETER
24 : VARIABLE DIAMETER PULLEY
25 : MOTOR
26 : MOTOR
27 : RECEIVER A (7.1ft³)

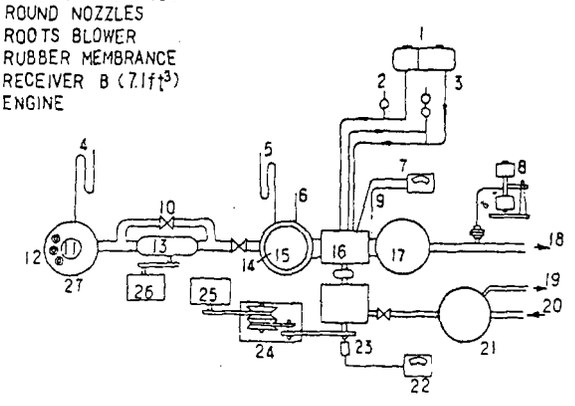

Fig. A-1 - Test equipment used

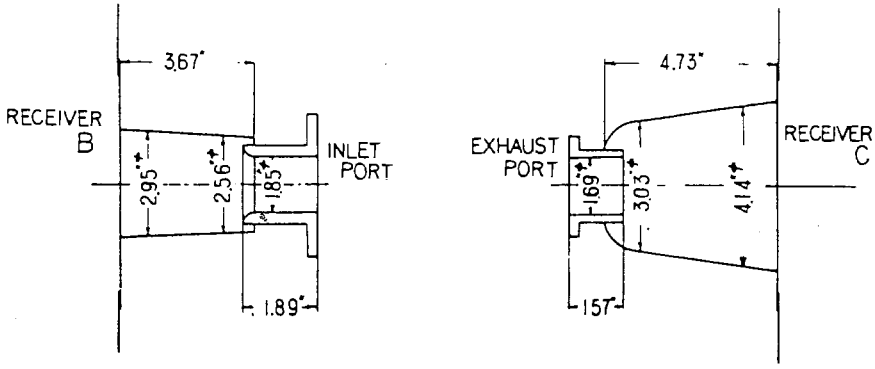

Fig. A-2 - Inlet and exhaust ducts in detail

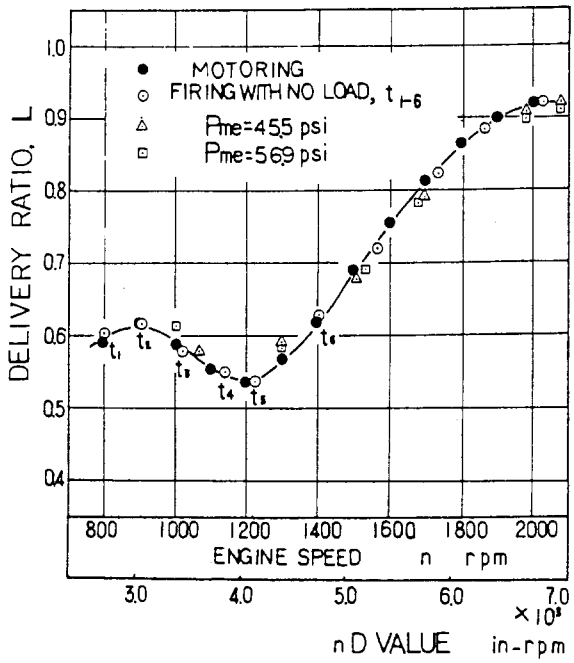

Fig. A-3 - Relation between delivery ratio and engine speed, in piston-valve inlet port engine. Notations t_1 - t_6 correspond to indicator diagram in Fig. 17

PART 2

CASE OF PISTON-VALVE INLET PORT ENGINE

THE OUTPUT CHARACTERISTICS of small crankcase-scavenged two-stroke cycle engines with the same scavenging system depend mainly on the delivery ratio. When there are no tuning effects from the inlet and/or exhaust pipe systems, the delivery ratio characteristics of such engines may be obtained approximately by motoring. The authors have reported (1)* the relations between the delivery ratio and engine speed for the case of a rotary disc valve inlet port engine.

In this Part, the same relations were investigated under motoring conditions with a conventional piston-valve inlet port engine by varying the angle area and the timing of the inlet port.

EQUIPMENT USED AND TEST PROCEDURES

The general specifications of the engine and equipment used are shown in Table 3 and Fig. 19. In order to avoid the tuning effects from the inlet and/or exhaust pipe systems on the delivery ratio characteristics, the exhaust port opened to the atmosphere through a short duct with a large cross-sectional area, as illustrated in Fig. 20. The inlet port opened directly into receiver C where the pressure was always kept equal to that of the atmosphere by a Roots blower equipped with a bypass valve. The air flow rate to the engine was measured by round nozzles (0.59 in.ϕ, 0.47 in.ϕ) (2) attached to the surface of receiver A. To ensure the correct opening and closing of the ports, the diameter of the piston (which was substituted for the one with no pin offset) was machined to a diameter equal to that of the piston skirt over its total length. The inlet port was varied by changing cylinder liners; the cylinders had different inlet ports but the same scavenging and exhaust ports as indicated in Fig. 21.

*Numbers in parentheses designate References at end of part 2.

The inlet port angle area of 102 deg-in.^{2} was nearly the same as the original and is denoted as Fia. Two methods of varying the inlet port with engine speed are practical: varying the port width keeping the port height constant, or varying the port height keeping the port width constant. Table 4 shows the relative width of the port in relation to the cylinder periphery and the relative height of the port in relation to the stroke at each different angle area from 1/5 Fia to 5/5 Fia. In the table, since the port width with a relative height lower than 24.7% in (a) and with a relative width wider than 39.8% in (b) overlaps the scavenging port in width, the inlet

Table 3 - General Specifications of Tohatsu T52D Engine

Type	Air-cooled, sigle-cylinder, Schnürle-scavenged, two-stroke cycle gasoline engine
Cylinder bore × stroke	2.04 in. ×2.28 in.
Cylinder volume	7.52 in.^{3} (123cc)
Rated output	10.3 hp/6700 rpm
Compression ratio	7.8:1
Crankcase compression ratio	1.37:1
Scavenging port	Opened 59.5 deg bbdc, closed 59.5 deg abdc, angle area - 59.6 deg-in.^{2}
Exhaust port	Opened 78.5 deg bbdc, closed 78.5 deg abdc, angle area - 107 deg-in.^{2}
Reduced angle area of scavenging and exhaust ports	46.6 deg-in.^{2}
Inlet port	Variable by changing cylinder liners

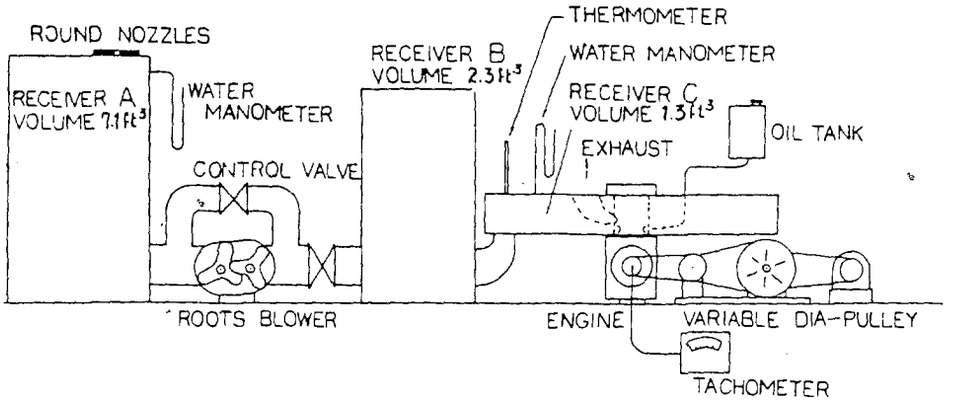

Fig. 19 - Test equipment used

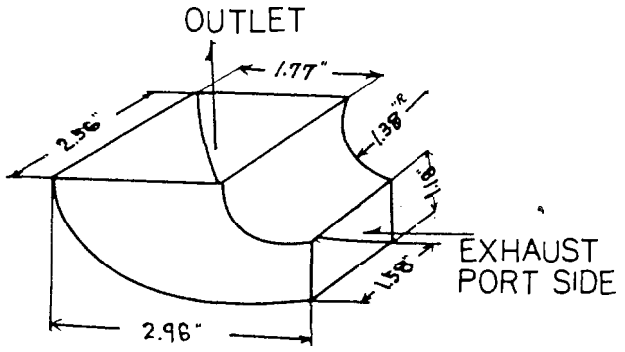

Fig. 20 - Exhaust duct in detail

port was divided into two halves. The other half was located beneath the exhaust port, as cylinder liners (b) and (c) in Fig. 21 indicate. As there was no inlet duct, the port width was taken along the cylinder periphery (that is, arc length), as illustrated in Fig. 22. To minimize the effect of thickness (3), the edges of the inlet ports and the bottom end of the piston skirt were finished as illustrated in Fig. 22.

Fig. 23 shows the relationship between the uncovered inl port area and the crank angle with different port configurations having the same angle area Fia. Fig. 24 shows the relation between the relative height and the relative width of the inlet port at Fia. In Fig. 24, when the relative heigh is reduced from 30% to 20%, the relative width increases

Table 4 - Inlet Port Conditions Tested

(a) Width of Inlet port (%) of Cylinder Periphery When Changing Angle Area, Keeping Port Height Constant (Nondimensional inlet port angle area Fia* = 0.121)

Port Height, H, %	Port Height, H, in.	1/5 Fia	2/5 Fia	3/5 Fia	4/5 Fia	5/5 Fia
35.3	0.81	4.6	9.1	13.7	18.2	22.8
30.0	0.69	5.9	11.8	17.6	23.5	29.4
24.7	0.56	8.0	15.9	23.9	31.8	39.8
21.4	0.49	9.7	19.4	29.1	38.8	48.5
19.7	0.45	11.3	22.5	33.8	45.0	56.3

(b) Height of Inlet Port (%) of Piston Stroke When Changing Angle Area, Keeping Port Width Constant (Nondimensional inlet port angle area Fia* = 0.121)

Port Width, B, %	Port Width, B, in.	1/5 Fia	2/5 Fia	3/5 Fia	4/5 Fia	5/5 Fia
56.3	3.62	6.7	10.7	14.1	17.1	19.7
48.5	3.12	7.4	11.9	15.5	18.6	21.4
39.8	2.56	8.5	13.6	17.6	21.4	24.7
29.4	1.89	10.3	16.6	21.5	26.0	30.0
22.8	1.47	12.2	19.5	25.3	30.5	35.3

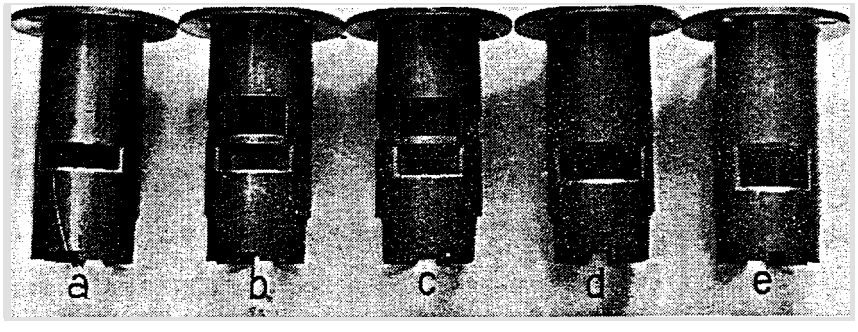

Fig. 21 - Cylinder liners having different inlet ports of constant angle area Fia = 102 deg-in.^{2}

m 30% to 56% which is impracticable unless the port is vided into two halves. The A and B marks in the figure dicate the tested range of port widths and heights. The ndimensional inlet port angle area, Fia,* is defined in pendix B of this part of the paper.

SCUSSION OF RESULTS

RELATION BETWEEN DELIVERY RATIO AND ENGINE EED - Figs. 25-27 show delivery ratio versus engine speed.

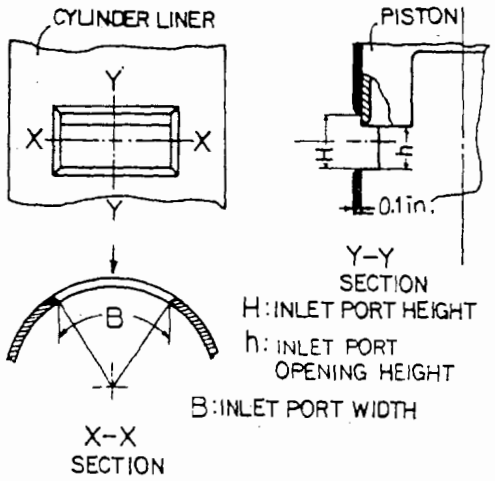

Fig. 22 - Inlet port in detail

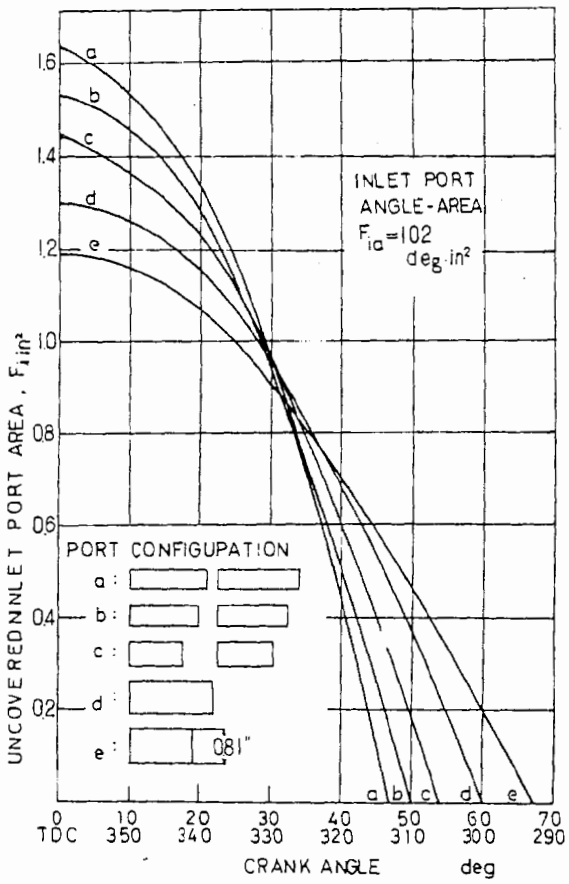

g. 23 - Relation between uncovered inlet port area and ank angle (all curves (a-e) have the same angle area)

In each figure, inlet ports with different configurations having the same angle area are illustrated. Fig. 25 covers the case of the largest angle area Fia. In Figs. 26(a)-(e) the inlet port was varied by changing the port height with a constant port width, while in Fig. 27 the inlet port was varied by changing the port width with a constant port height. In each figure, the engine speed which produced the maximum delivery ratio, hereafter denoted as n_o, shifted to a higher speed with an increase of inlet port angle area. As is known, at a certain inlet port angle area, when the engine speed is higher than n_o, the angle area becomes inadequate, that is the inlet port closes before the inlet process finishes. On the other hand, when the engine speed is lower than n_o, the angle area is too large to check the reverse flow of the

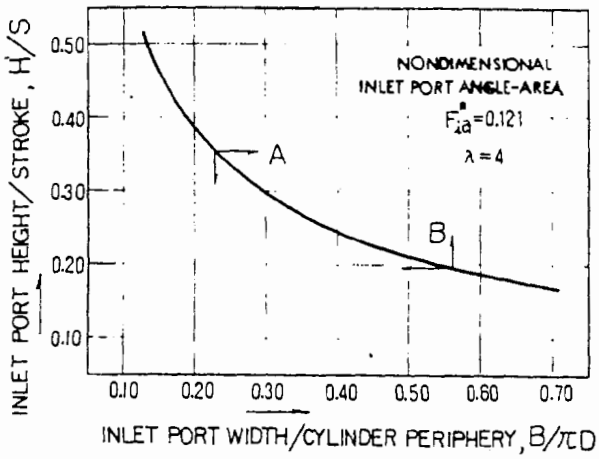

Fig. 24 - Relation between port width and port height at constant angle area (λdenotes ratio of connecting rod length and crank radius)

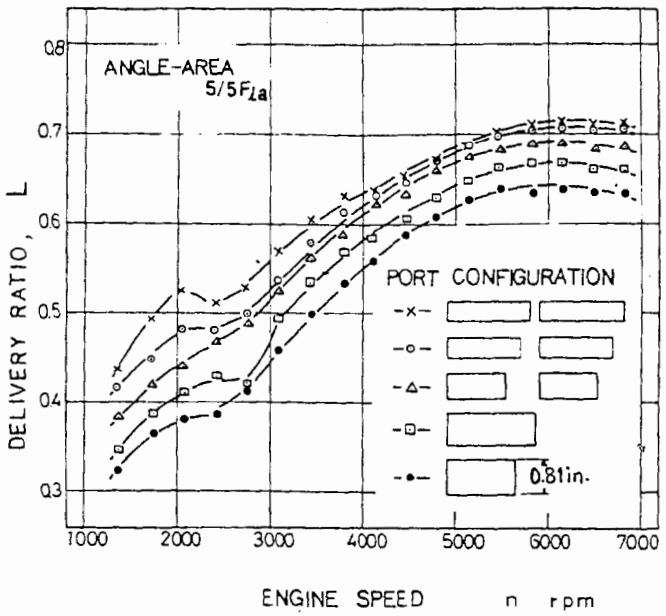

Fig. 25 - Relation between delivery ratio and engine speed, case of largest angle area

air from the crankcase. Also, each figure shows that when the inlet port angle areas were identical, a lower and wider port (resulting in a longer effective crankcase stroke) produced a larger delivery ratio over the entire engine speed range.

Fig. 28 shows superimposed envelopes representing the delivery ratio curves of Figs. 25-27. Shown are the limiting delivery ratio curves when the angle area and timing of the inlet port are changed. Also, nD values (n = engine speed in rpm, D = cylinder bore in in.) are indicated. Fig. 28 shows that when angle area of inlet port was varied in accordance with the change of engine speed to improve the delivery

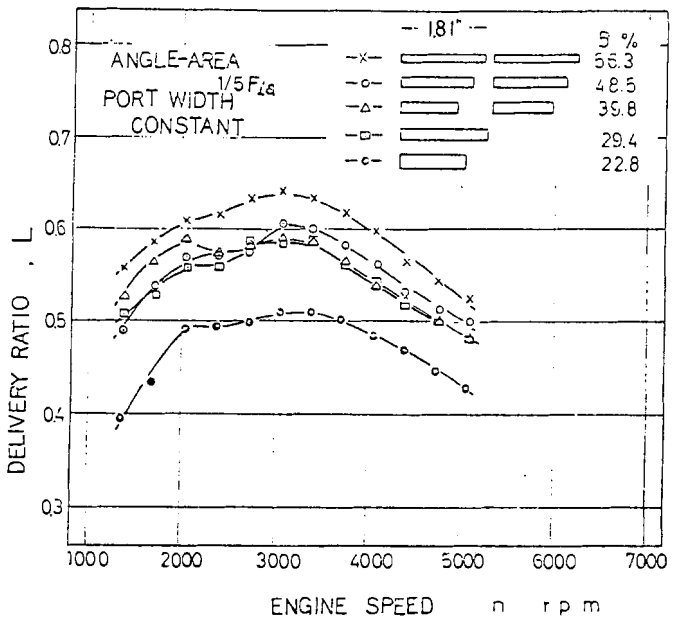

Fig. 26 (a) - Relation between delivery ratio and engine speed

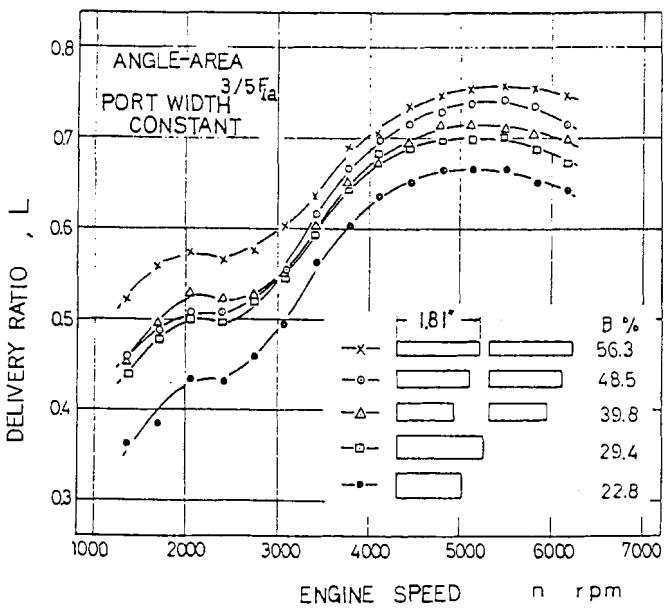

Fig. 26 (b) - Relation between delivery ratio and engine speed

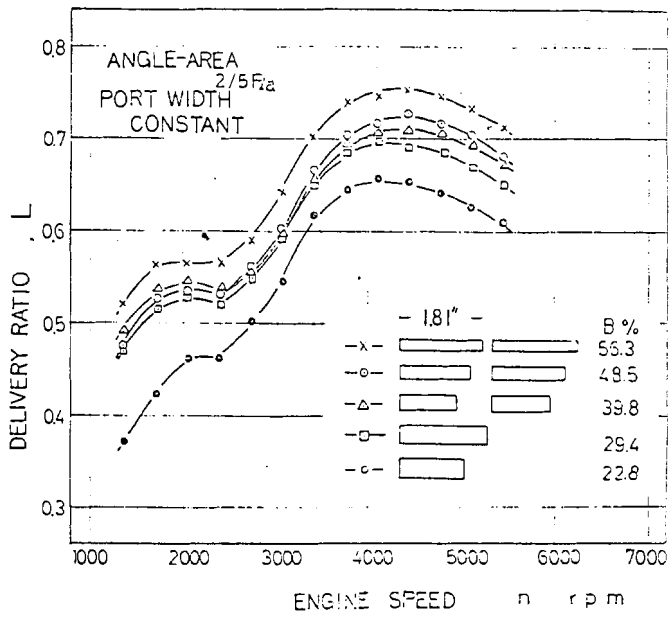

Fig. 26 (c) - Relation between delivery ratio and engine sp

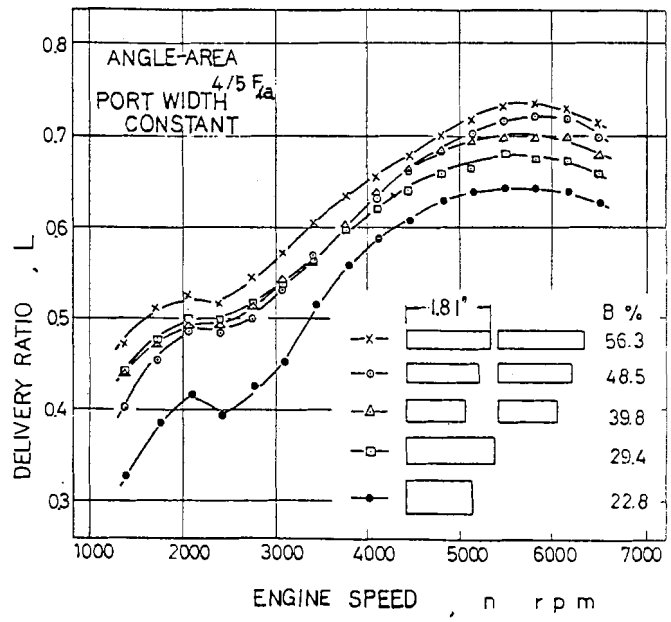

Fig. 26 (d) - Relation between delivery ratio and engine spe

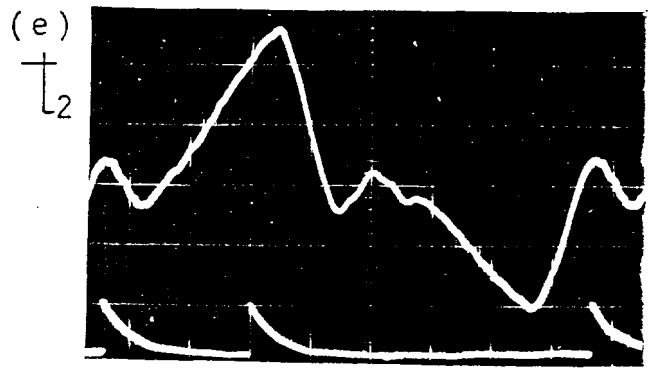

Fig. 26 (e) - Representative crankcase indicator diagram

tio characteristics, it was better to vary the port height eeping the port width constant than to vary the port width eeping port height constant. In Fig. 28, the delivery ratio urve of the inlet port with a 30% relative height and 4/5 a angle area, which is nearly the original design, is indiated by -⊡- and the curve of 17.1% relative height, which the lowest port with same angle area, is indicated by -X-. From this figure, it follows that by varying only e inlet port, some improvement of delivery ratio characristics can be expected. Especially when the inlet port eight is varied keeping the port width constant with the change of engine speed, the delivery ratio characteristics in the middle and low speed ranges can be improved significantly.

Fig. 29 shows the relation between the maximum delivery ratio L_{max}, which is given from each delivery ratio curve in Figs. 25-27, and the effective crankcase stroke. Solid lines represent a constant port width and dashed lines a constant port height. Noting from Figs. 25-27 that when the delivery ratio curve had a large L_{max} the whole curve was higher over the entire engine speed range, L_{max} is

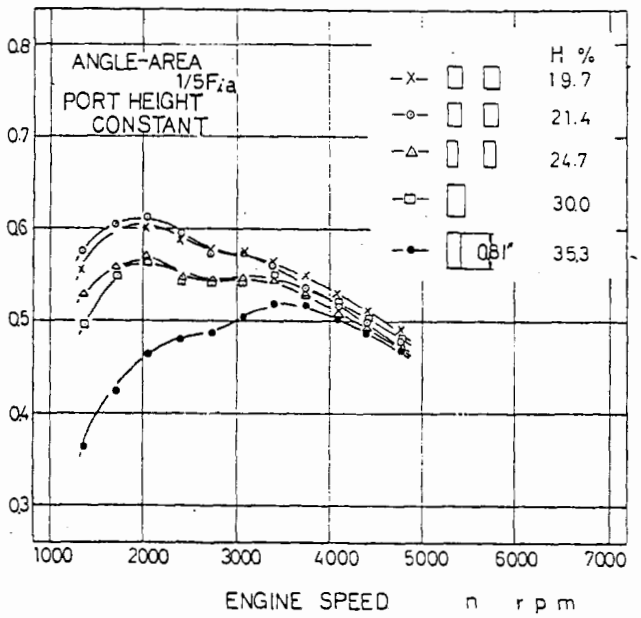

g. 27 (a) - Relation between delivery ratio and engine eed

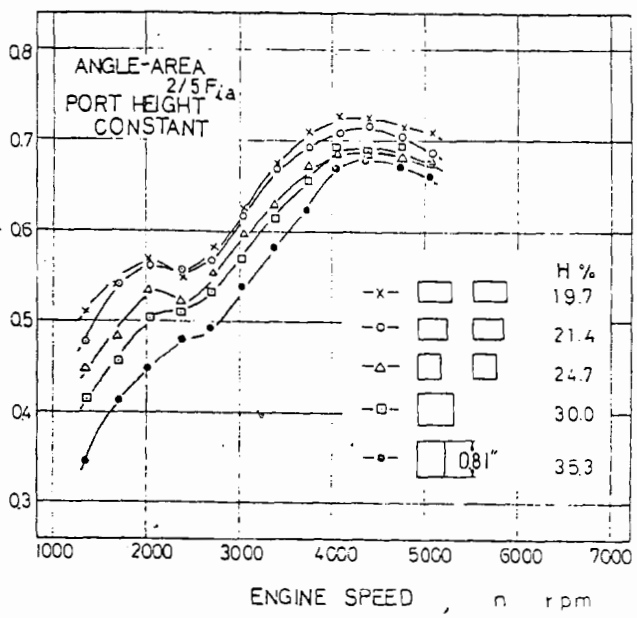

g. 27 (b) - Relation between delivery ratio and engine eed

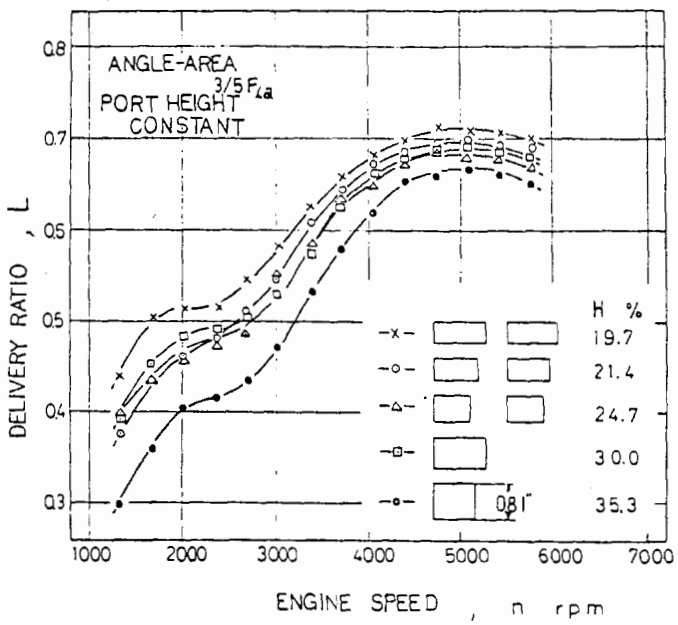

Fig. 27 (c) - Relation between delivery ratio and engine speed

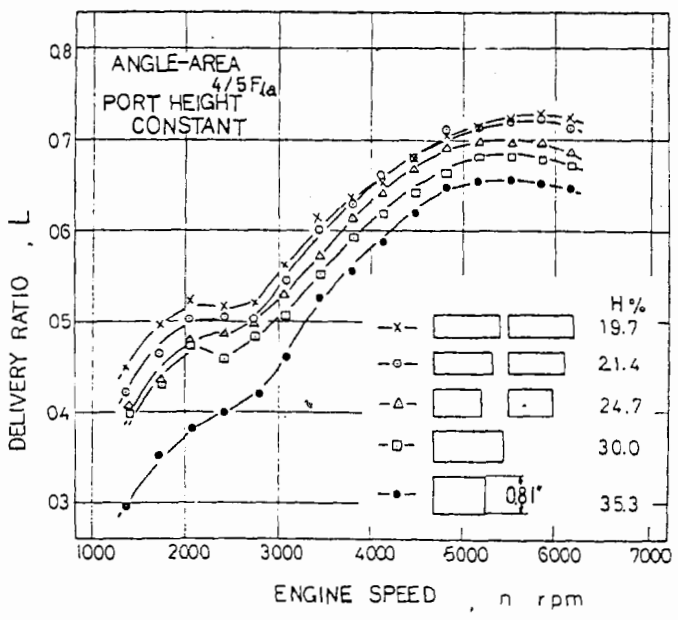

Fig. 27 (d) - Relation between delivery ratio and engine speed

plotted. Fig. 29 indicates that when the angle area of the inlet port was the same, L_{max} increased almost in proportion to the increase in effective crankcase stroke. Comparing the dashed lines with the solid lines, it is clear that with the same angle area, a lower and wider inlet port (which causes a longer effective crankcase stroke) produced a larger delivery ratio. Noting that the delivery ratio curves with a larger angle area than 3/5 Fia were nearly superimposed, it may be said that when angle area is large enough, L_{max} is almost determined by the effective crankcase stroke.

In case of the surves with solid lines, L_{max} became a maximum when the angle area was about 3/5 Fia, while in case of the dashed lines, L_{max} became a maximum at about 4/5 Fia. The reason may be stated as follows: when the port height is varied keeping the port width constant, a longer effective crankcase stroke is available, which causes a higher crankcase compression ratio and thus less inlet port angle area is needed.

As the engine used had 46.6 deg-in.^{2} reduced angle area of the scavenging and exhaust ports, the value of (angle area of the inlet port which produced maximum L_{max}, that is, optimum angle area of the inlet port)/(reduced angle area of the scavenging and exhaust ports) was 1.31 and 1.75 in each case, respectively.

Little hills are observed on the delivery ratio curves of Figs. 25-27 in the low engine speed range. As this phenomenon is already discussed in detail in Part 1 of this paper, explanation of it is omitted here.

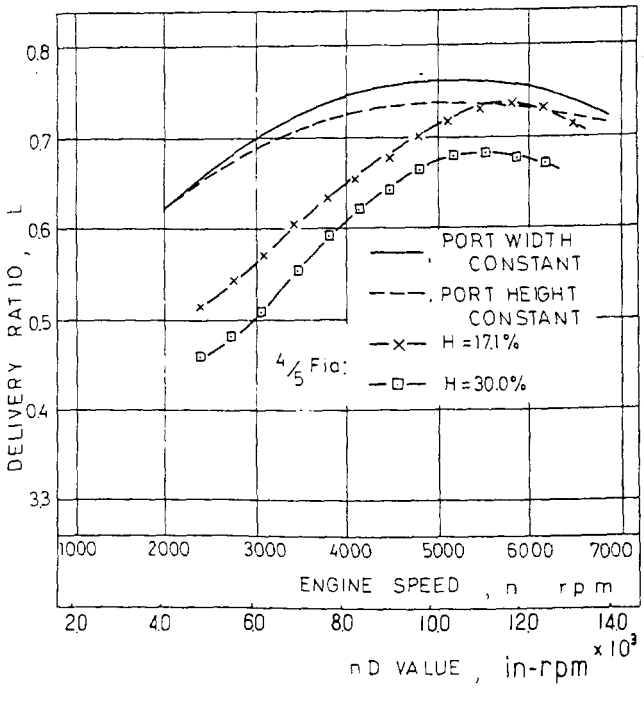

Fig. 28 - Relation between delivery ratio and engine speed (comparison of the limiting delivery ratio curves between port width constant and port height constant)

Discussions of the pressure indicator diagrams calculated in the crankcase with variable inlet port height were previously reported (4, 5). So, in this paper, attention is directed to another important factor which affects delivery ratio -- the flow coefficient of the inlet port.

ANALYSIS OF FLOW COEFFICIENT OF INLET PORT

In order to understand better the test results mentioned above, the authors think it is necessary to take a close look at the flow coefficient of inlet ports with different configurations. In view of the fact that L_{max} increases with an increase in effective crankcase stroke (Fig. 29), attention is directed to the flow coefficient of the low, wide inlet port. Compared with the case of a poppet valve, the flow coefficient of this type of inlet port has been scarcely discussed. To know the effect of the port configuration and engine speed on the flow coefficient, a flat plate model of the inlet port and cylinder liner inlet port were used for testing.

TEST EQUIPMENT USED AND TEST PROCEDURE - The test equipment used is illustrated in Fig. 30. A flat plate model of the inlet port shown in Fig. 31 or a cylinder liner inlet port was attached to the surface of receiver B'. The air flow rate was measured by round nozzles (0.71 in.ϕ, 0.59 in.ϕ, 0.45 in.ϕ) at receiver A. The flow coefficient

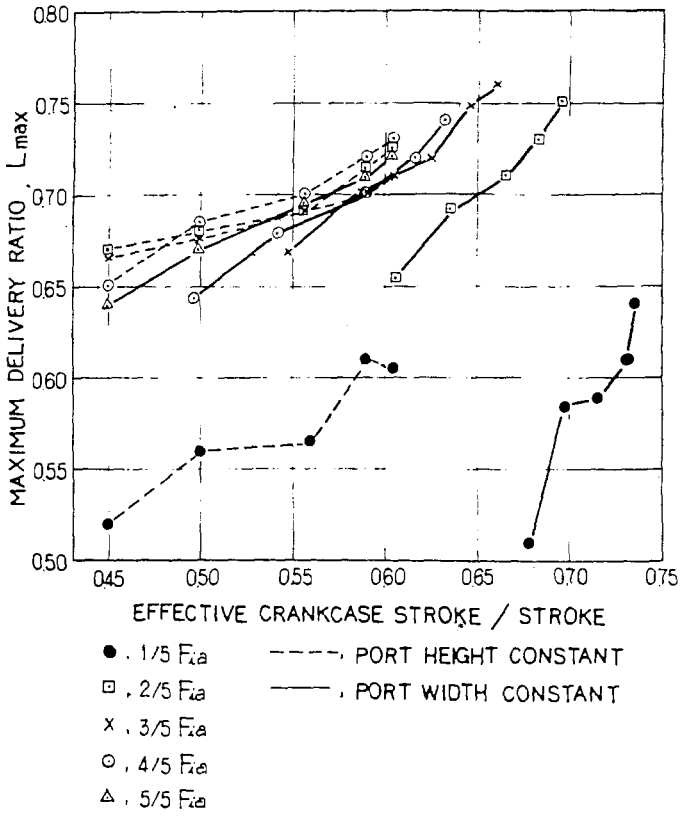

Fig. 29 - Relation between maximum delivery ratio and effective crankcase stroke. Dashed lines - when port width is changed at constant angle area. solid lines - when port height is changed at constant angle area

was defined as the ratio of the measured flow to the theoretical flow through the model or the cylinder liner inlet port. The flow rate was varied at each port configuration by changing the pressure difference across receiver B' between 3.9 and 15.8 in. water manometer. As is known from the literature (6-9), this small pressure difference did not cause any difference in the measured flow coefficients.

FLAT PLATE MODEL OF THE INLET PORT - As illustrated in Fig. 31, the edges of port were rounded to a quadrant arc, which was varied by changing the thickness of the plate to determine the effect of the rounded edges on the flow coefficient. Although several back plates with different thicknesses were tested, the influence of this thickness on the flow coefficient was not significant; therefore, the same back plate with a thickness of 0.1 in., which corresponded to the thickness of the piston skirt of the engine, was used throughout the entire experiment. Two types of ports with 1.18 in. width and 0.59 or 1.18 in. heights were used with the following plate thicknesses (that is, with the following quadrant arc radii): 0.1, 0.2, 0.3, and 0.4 in. In each case, the back plate was positioned to vary the port opening height.

CYLINDER LINER INLET PORT - The cylinder liners shown in Fig. 21 were used. As illustrated in Fig. 30(b), piston was positioned in the cylinder to vary the port opening height. The measured flow coefficients were compared with the case of the flat model port and also with those measured under dynamic conditions.

RECIPROCATING ENGINE INLET PORT - The relations between the flow coefficients measured under static and dynamic, that is, reciprocating, conditions were investigated using the test equipment illustrated in Fig. 30 (a).

Air flow from the Roots blower passed through receiver B' and was led to receiver C', while the model port at receiver B' was sealed. The inlet port in the cylinder liner opened directly into receiver C'. The crankcase had several outlet ports of 5.6 sq in. total area leading to the atmosphere. The air flowed from receiver C' into the crankcase through the cylinder liner inlet port, then out into the atmosphere. As the angle area of the inlet port almost coincided with the reduced angle area of the inlet port and the outlet ports in the crankcase, the authors thought it was permissable to ignore the pressure fluctuations in the crankcase.

If the air flow rate per cycle into the crankcase is expressed as Gc, then

$$Gc = \mu dm \int_{\theta_{io}}^{\theta_{ic}} F_i(\theta) \cdot d\theta/(\theta_{ic} - \theta_{io}).$$

$$\sqrt{\frac{2g\kappa}{\kappa - 1} \cdot \frac{P_{c'}}{V_{c'}} \left[\left(\frac{P_{o'}}{P_{c'}} \right)^{2/\kappa} - \left(\frac{P_o}{P_{c'}} \right)^{(\kappa+1)/\kappa} \right]} \cdot \Delta t \quad (1)$$

where

F_i = Inlet port area
θ = Crank angle
g = Acceleration due to gravity

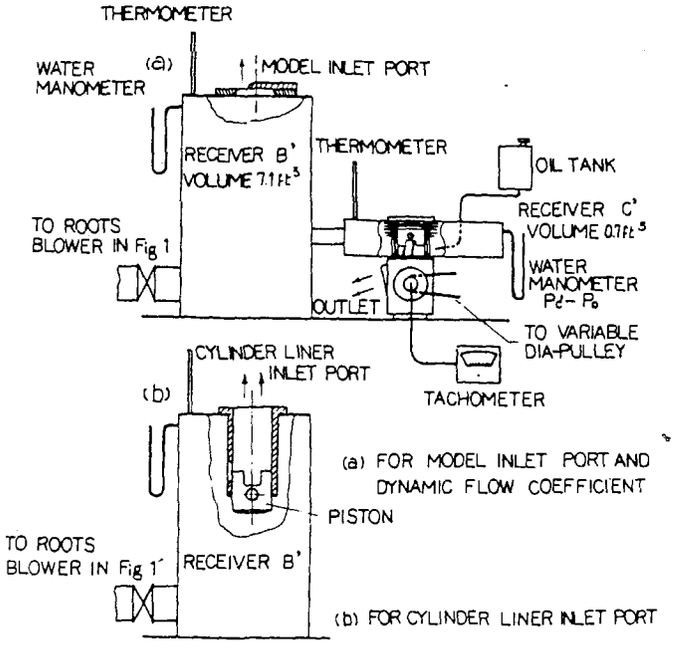

Fig. 30 - Test equipment used for measuring the flow coefficient of inlet port

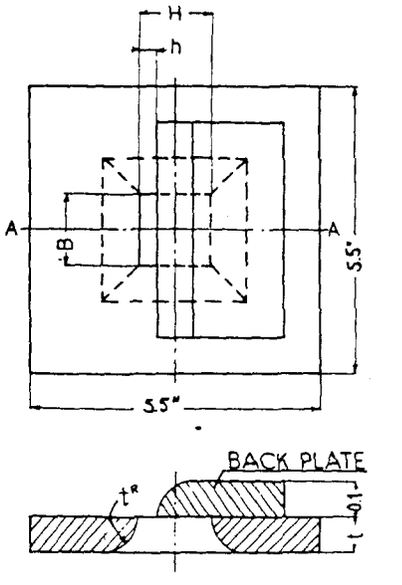

t : 0.1 , 0.2 , 0.3 , 0.4 in.
h : INLET PORT OPENING HEIGHT
H : INLET PORT HEIGHT
B : INLET PORT WIDTH

Fig. 31 - Model of inlet port in detail

κ = Specific heat ratio

$P_{c'}$ = Pressure in receiver C'

P_o = Ambient pressure

$V_{c'}$ = Specific volume of air in receiver C'

Δt = Port opening period of inlet port

θ_{io}, θ_{ic} = Opening and closing of inlet port, respectively

μdm is called the dynamic mean flow coefficient in this paper.

$\int_{\theta_{io}}^{\theta_{ic}} F_i(\theta) \cdot d\theta/(\theta_{ic} - \theta_{io})$ indicates the mean inlet port area during the port opening period.

The pressure difference across receiver C' was varied between 3.9 and 23.6 in. water manometer, while the engine was driven through the variable diameter pulley at 1700-6000 rpm. At each condition, μdm was calculated using the measured values from Eq. 1. The relation between the static flow coefficient μs and the dynamic mean flow coefficient μdm is written as follows:

$$\mu dm \int_{\theta_{io}}^{\theta_{ic}} F_i(\theta) \cdot d\theta = K \cdot \int_{\theta_{io}}^{\theta_{ic}} \mu s(\theta) \cdot F_i(\theta) \cdot d\theta \qquad (2)$$

where:

$$\int_{\theta_{io}}^{\theta_{ic}} \mu s(\theta) \cdot F_i(\theta) \cdot d\theta / \int_{\theta_{io}}^{\theta_{ic}} F_i(\theta) \cdot d\theta = \mu sm \qquad (3)$$

Eq. 3 shows the static mean flow coefficient. The ratio of μdm and μsm is denoted as K, and is called the dynamic factor in this paper. That is,

$$\mu dm/\mu sm = K \qquad (4)$$

DISCUSSION OF RESULTS -

Static Flow Coefficient -

1. Effect of the port configuration and the rounded edges (quadrant-arc sections) of the inlet port on the flow coefficient.

Fig. 32 shows the relationship between the static flow coefficient μs and the relative height of the inlet port opening in relation to the port width h/B. From each μs curve, it follows that μs was larger near the beginning of port opening and decreased as the port opening height, h, increased. The results were the same as those of List, Niedermayer (10) and Benson (11), who measured the μs values at the scavenging and exhaust ports which had guiding surfaces, such as the piston crown and the scavenging and exhaust ducts. It also correlated well with the results of Suda (4), who measured the μs values of an inlet port with a duct, and those of Tanaka (12), Kastner (8), and Pope (9) who measured the μs values of the poppet inlet valves. In the case of the poppet valve, Tanaka (13) took photographs of the air flow around the inlet valve, and Kastner (8) investigated the air flow on a two-dimensional model of the inlet port using a pitot tube. Both results showed that the flow separation from the guide surface increased with an increase in port opening height. Annand (8) explained that with poppet valv the viscous effects in the gap suppressed the flow separation from the guide surface when the port opening height was low.

It is generally acknowledged that the flow coefficient is the product of the velocity coefficient and the contractio coefficient. The velocity coefficient is thought to decreas with small nozzles because of the increase in the friction loss due to the viscous effect. On the other hand, the contraction coefficient is due to three-dimensional effects (14) an is said to increase as a result of compressibility with an increase in pressure ratio, as the test results of Ramamoorty (15) with quadrant arc nozzles and Perry (14) with sharp-edge orifices showed. Taking these facts into account and noting the μs curves in Fig. 32 μs increases with a decrease in h/B, that is, a narrow port has a larger μs. This means that the viscous effects in the gap, which may suppress the flow separation, are not so significant as to decrease the velocity coefficient, but the increase in contraction coefficient affects the increase in μs. The increase in contraction coefficient with the decrease in h/B may be partly due to the reduction of flow separation and partly to the

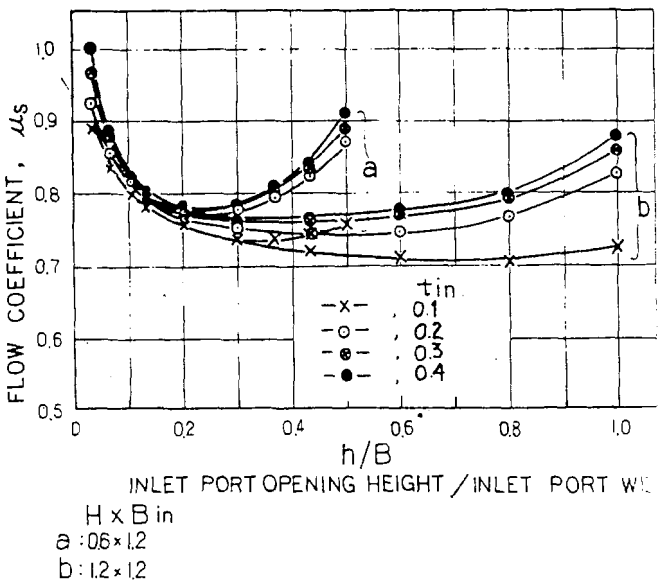

Fig. 32 - Relation between flow coefficient and inlet por configuration (influence of rounded edges on flow coefficient)

change of flow patterns from three-dimensional to nearly two-dimensional, that is, the effect of the side walls on the flow becomes less with a decrease in the port opening height. This is also verified by noting the fact that when the port opening height was the same, the wider port had a larger μs, as is indicated later in Fig. 35.

All of the μs curves in Fig. 32 decrease smoothly with an increase in h and no singular points are seen on the curves, as are usually observed in the case of poppet valves. Considering the test results of Tanaka and Kastner, it seems that the flow separation point, that is, the front of the free stream line, shifts smoothly because of the rounded edges of the inlet port, as illustrated in Fig. 31.

In the actual engine, when the inlet port opens, the pressure difference between the crankcase and the atmosphere is much greater than in these tests. Therefore, because of the increase in contraction coefficient caused by the compressibility of the air, the actual curves may be higher than the measured values in the neighborhood of port opening.

The effect of the rounded edges of the quadrant arc section was significant. Although a larger radius of curvature produced a larger μs in the figure, by noting that there was little difference in the μs curves between plate thicknesses t = 0.3 and t = 0.4 in., t/(Width of inlet port) = 0.3 seems to be an appropriate value.

Here, it should be noted that μs increased again when the port opening height, h, approached the port height, H. This is significant, as μs is large when the uncovered port area is large enough. This causes a larger effective inlet port angle area. As illustrated in Fig. 23, a wider and lower inlet port had a larger maximum port area than a narrower and higher inlet port for the same angle area. Moreover, the increase in μs around top dead center, that is, near maximum port opening area, was more remarkable for such a port. These facts indicate that a wider and lower inlet port is more desirable for obtaining a larger effective angle area.

This increase in μs may be caused by the effect of the rounded upper edge of the port. Fig. 33 shows two types of ports having the same rounded edges but different port heights. In Figs. 33(a) and 33(b), both pistons had the same port opening height, that is, both ports had the same port opening area. In the case of Fig. 33(a), the sharp bottom edge of the piston skirt may have caused a significant contraction of flow, while in Fig. 31(b), it may have been less because of the rounded upper edge. This caused a difference in μs. When piston was located to give full port opening in Fig. 31(b), the difference in μs became more remarkable. In Fig. 32, the point of 0.5 in relative port height h/B corresponds to this particular case.

In short, a wider and lower inlet port having rounded edges, especially a rounded upper edge with large radius of curvature, produced a larger μs throughout the inlet port opening period.

2. Relation between the flat plate model and the cylinder liner inlet port.

Fig. 34 shows μs for the same size inlet ports, (a) with the model and (b) with the cylinder liner. The difference was, as shown in Fig. 22, the width of the inlet port; in the case of the cylinder liner, the width was measured along the cylinder periphery, causing a shorter effective port width. The configuration of the port was nearly the original. The width of the port reached about 28% of the cylinder periphery, which was about the maximum value possible to avoid overlap with the scavenging ports. In this case, the difference in μs between the model and the cylinder liner ports may be most remarkable. As is seen in the figure, the difference occured as the port opening height increased, and it became the largest at the fully open position. Comparing μsm calculated from μs, μsm became 0.74 and 0.68 to each case, respectively, that is, the difference in effective angle area between them was about 9%.

Furthermore, using the measured μsm value of 0.70 obtained by Suda (4) with same engine but having an inlet duct (in this case, the width of port was measured perpendicular to the air flow or chordally), the effective angle area in both cases may be compared. μsm was 0.70 and 0.68; the port width was B' and B in each case, respectively,

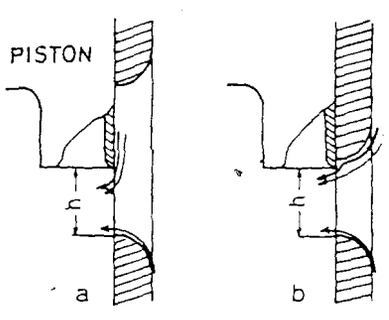

Fig. 33 - Influence of rounded upper edges on inlet flow

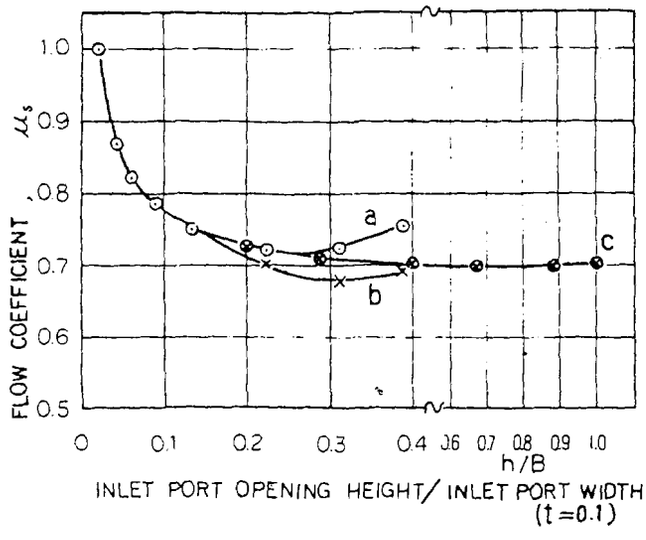

Fig. 34 - Relation between the flow coefficient and inlet port cofiguration (relation between cylinder liner inlet port and model of inlet port)

as indicated in Fig. 35. Thus, the ratio of effective port area in both cases was (0.68 × B)/(0.70 × B'). It follows that about an 11% increase in effective angle area is possible when using the port width along the cylinder periphery. This means that it is better, if possible, not to use an intake duct but to make the inlet port open directly into the air (as in this experiment) in order to increase the effective angle area with the same size of inlet port. In Fig. 34, the μs of a square port with the same width is also indicated.

3. Effect of a rounded bottom edge of the piston skirt on μs.

The μs values so far were measured using a piston skirt having a sharp bottom edge as illustrated in Fig. 36 (a).

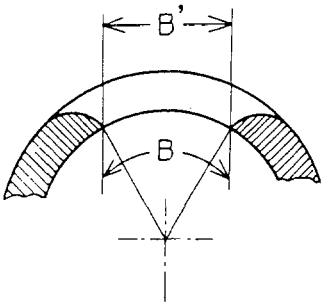

Fig. 35 - Port width, relation between arc B and chord B'

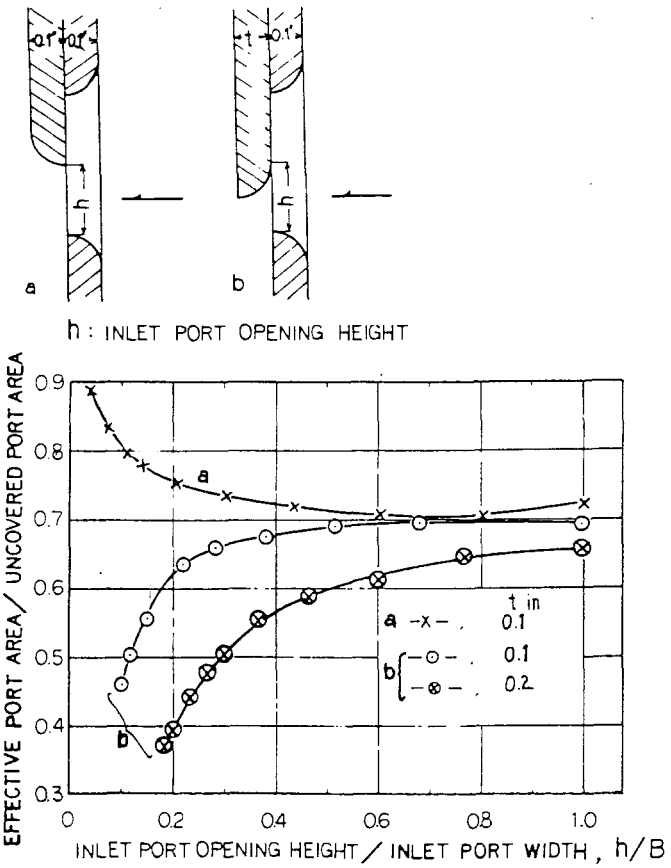

Fig. 36 - Relation between flow capability and inlet port configuration (influence of rounded bottom edge of piston)

Here, the effect of a rounded bottom edge, as illustrated in Fig. 36(b), on μs was investigated. In this case, the port opening height, h, should be taken as in Fig. 36, and since the term flow coefficient may not be appropriate, the ratio of effective port opening area to port opening area is used instead of μs. From Fig. 36 it follows that the larger the radius of curvature at the bottom edge of the piston skirt, the smaller the effective port opening area became.

Dynamic Flow Coefficient -

To understand the effect of dynamic (that is, reciprocating) conditions on the flow coefficients, the dynamic mean flow coefficients μdm were measured on the motored engine using the test equipment illustrated in Fig. 30(a). First, the static flow coefficient μs were measured with the same cylinder liners, selecting the three port configurations of Figs. 23(a), (d), and (e). All of these had the same angle area of Fia = 102 deg-in.^{2} (Fia = 0.121). The measured μs values are shown in Fig. 37, which shows that the wider port had a larger μs when the port opening height, h, was the same. Comparing the effective angle area, that is, static mean flow coefficient, using Fig. 23 μsm became 0.72, 0.68, and 0.62 for each of (a), (d), and (e), respectively. This means that a wider and lower port had a larger μsm when the angle area was the same.

Figs. 38 a-c show the μdm values measured. In each figure, μdm decreased with an increase in engine speed. This tendency was more remarkable when there was less pressure difference across the inlet port. When the engine speeds and the pressure differences were the same, a wider and lower port tended to have a larger μdm.

These facts indicate that μdm had a close relation to the inlet air velocity and the piston velocity, as illustrated in Fig. 39. So, the theoretical inlet velocity V_a caused by the pressure difference across the inlet port, and the mean piston velocity $\overline{V}_p$ while the inlet port was open were cal-

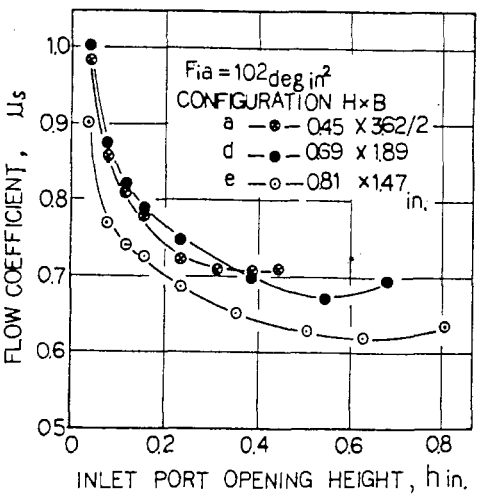

Fig. 37 - Relation between flow coefficient and inlet port opening height

culated with the following formulas:

$$V_a = \sqrt{\frac{2g}{\gamma_{c'}} \cdot (P_{c'} - P_o)} \qquad (5)$$

(theoretical inlet air velocity)

$$\overline{V}_p = 2H \Big/ \frac{\theta_{ic} - \theta_{io}}{360} \cdot \frac{60}{n} \qquad (6)$$

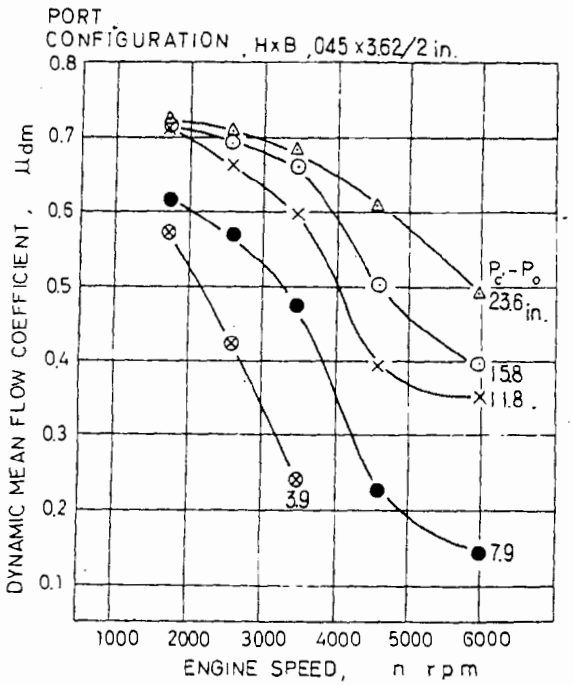

Fig. 38 (a) - Relation between flow coefficient and engine speed

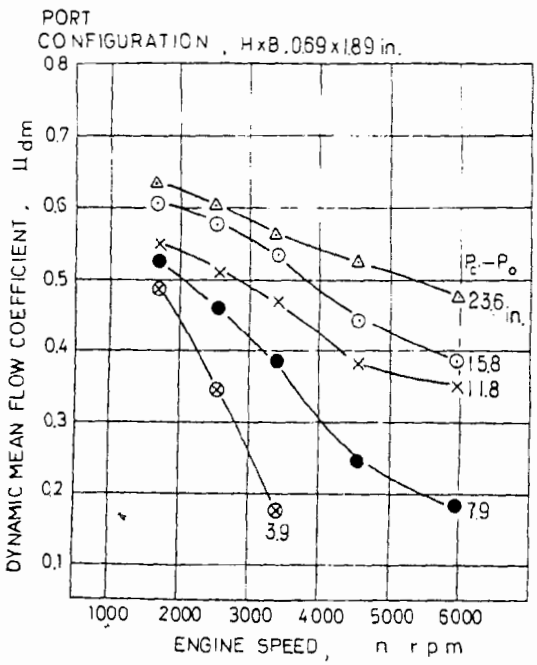

Fig. 38 (b) - Relation between flow coefficient and engine speed

(mean velocity of the piston during the inlet port opening period)

where:

$P_{c'} - P_o$ = Pressure difference between receiver C' and atmosphere

$\gamma_{c'}$ = Specific weight of air in receiver C'

g = Acceleration due to gravity

H = Inlet port height

$\theta_{ic} - \theta_{io}$ = Crank angle corresponding to inlet port opening period

n = Engine speed

Taking $V_a/\overline{V}_p$ as the abscissa, the measured μdm values were rearranged as shown in Figs. 40(a)-(c). These figures show all of the μdm values gathered on a certain curve in each case. Also μsm and K are indicated. As is seen, with an increase in $V_a/\overline{V}_p$, μdm approached μsm. In the case

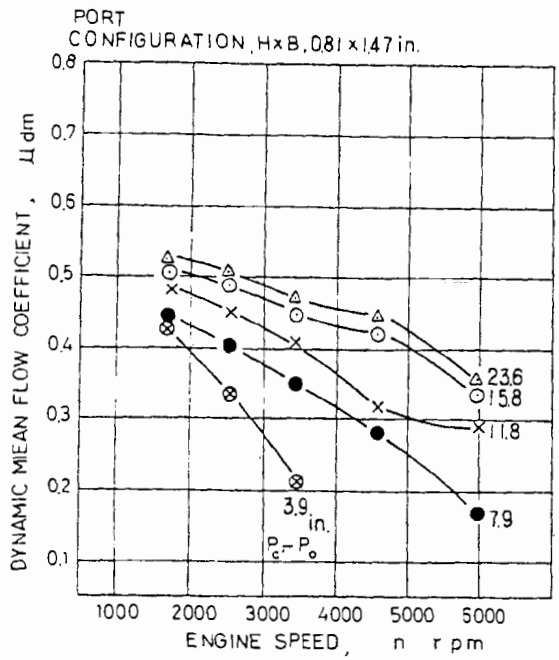

Fig. 38 (c) - Relation between flow coefficient and engine speed

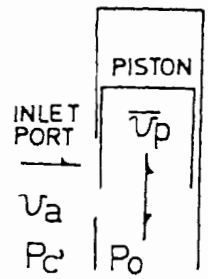

Fig. 39 - Relation between inlet velocity and piston velocity

of the lower and wider port, the approach was more rapid. Since an increase in $V_a/\overline{V}_p$ indicates a decrease in piston velocity, it seems to be natural that μdm approached μsm with an increase in $V_a/\overline{V}_p$.

In the case of port configuration (a), K was already unity at $V_a/\overline{V}_p = 30$. On the other hand, in the cases of (d) and (e), K was 0.94 and 0.80, respectively. Besides that, μsm was smaller than in the case of (a).

The results obtained may be explained as follows: in the case of a larger μsm, (that is, when the air flowed closely along the guide surfaces), the flow was more stable against external disturbances than in the case of a smaller μsm (that is, when the air flowed with separation having free stream lines). Moreover, as the lower port had a lower $\overline{V}_p$ at the same engine speed, the dynamic effect became less significant.

Therefore, when the angle area of the inlet port is fixed, it is better to use a wider and lower port in order to get a larger effective angle area, as the μdm value of such a port approaches a larger μsm value more quickly at smaller $V_a/\overline{V}_p$ values.

In case of the actual engine, the value of $V_a/\overline{V}_p$ is much larger than in these tests in most port opening periods, so the authors think it reasonable to use μsm instead of μdm in deciding the capability of air flow through these ports.

In contrast to the explanation of Kastner, even with the

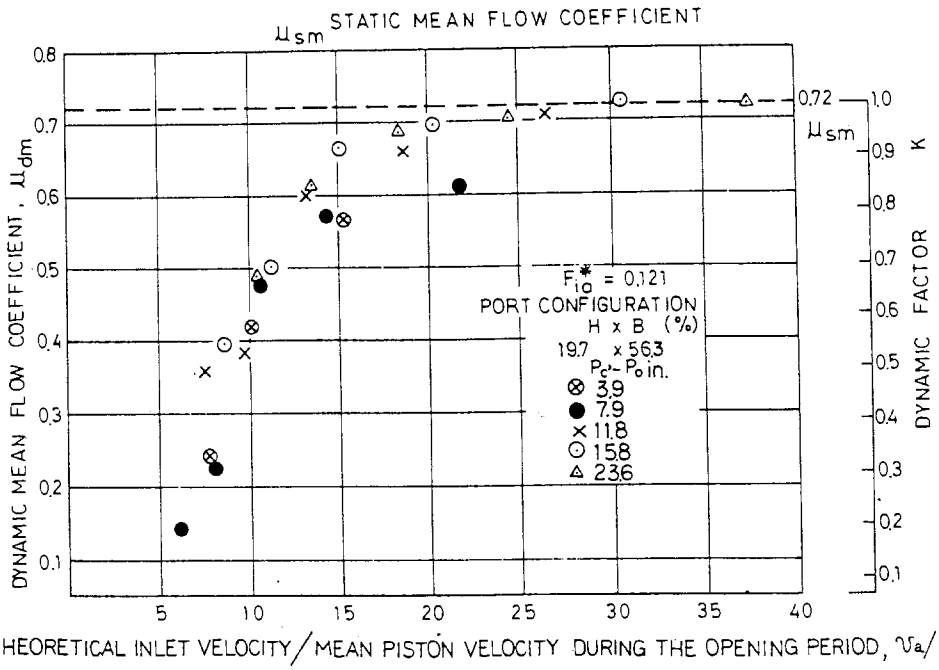

Fig. 40 (a) - Relation between dynamic mean flow coefficient μdm and $V_a/\overline{V}_p$

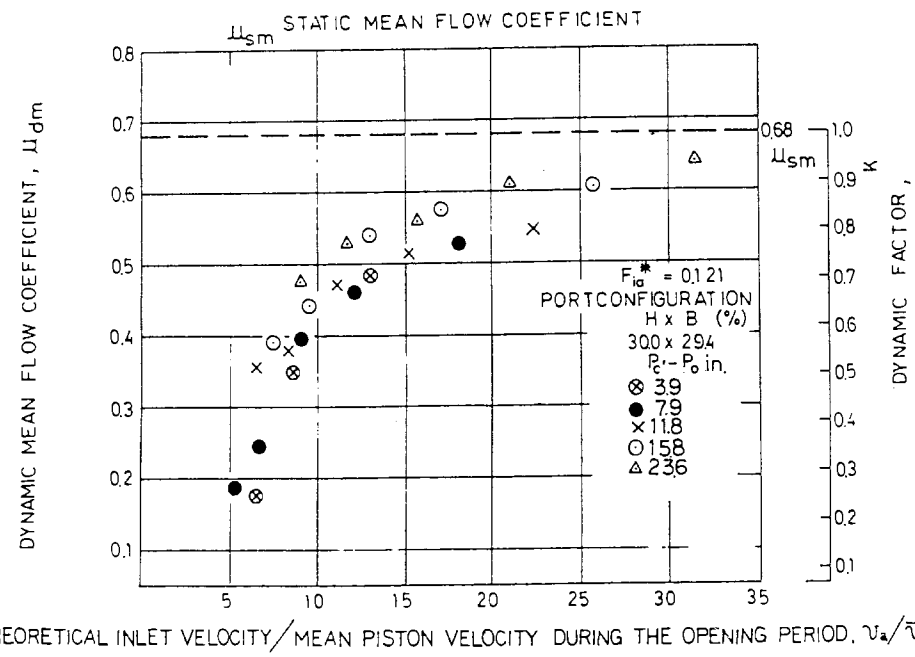

Fig. 40(b) - Relation between dynamic mean flow coefficient μdm and $V_a/\overline{V}_p$

test equipment used having no inlet duct, μdm decreased with an increase in engine speed. So, the decrease in μdm should be considered due to the loss of energy which is involved in accelerating the air regardless of the inlet duct or inlet passage.

From the above, it follows that the reason a lower and wider inlet port produces a larger delivery ratio is not only the longer effective crankcase stroke but also the increased flow coefficient.

CONCLUSIONS

By motoring an engine having a conventional piston-valve inlet port which had no tuning effects from the inlet and/or exhaust pipe systems, and by changing widely the angle area and timing of the inlet port, the relations between engine speed and delivery ratio were investigated.

At the same time, the flow coefficients of inlet ports with different configurations were investigated under static and dynamic conditions. The results obtained were:

1. With an increase in inlet port angle area, the engine speed n_o which produces the maximum delivery ratio increases, and at a certain angle area the delivery ratio obtains its maximum value. This optimum angle area differs, depending upon whether the port width is varied keeping the port height constant or the port height is varied keeping the port width constant. In the latter case, the optimum angle area is smaller.

2. The maximum delivery ratio varies when the port height and port width are changed keeping the angle area constant. A lower and wider inlet port produces a larger delivery ratio, that is, the maximum delivery ratio is nearly in proportion to the effective crankcase stroke.

3. A lower and wider inlet port has a larger static mean flow coefficient.

4. The radius of curvature, which corresponds to about 30% of the port width at the port edges, is favorable for a larger flow coefficient. Especially, a rounded upper edge of the inlet port is significant in increasing the flow coefficient at nearly complete port opening.

5. If possible, it is better to use the inlet port arrangement which utilizes the cylinder periphery as effective port width to increase the effective port area.

6. A rounded bottom edge of the piston skirt decreases the effective port area.

7. Usually, the dynamic mean flow coefficient μdm of the inlet port is smaller than the static mean flow coefficient μsm. The smaller the pressure difference across the inlet port and the higher the engine speed, the more significant the difference between them becomes.

8. Plotting μdm as the ordinate and the ratio of the theoretical inlet velocity caused by the pressure difference across the inlet port and the mean piston velocity during the inlet port opening period $V_a/\overline{V}_p$ as the abscissa, almost all μdm gather on a certain curve. In the case of the wider and lower inlet port, μdm approaches μsm at small values of $V_a/\overline{V}_p$.

9. In judging the air flow capability of this type of inlet port, it seems to be reasonable to use μsm instead of μdm.

Therefore, the authors would like to propose using the widest port possible varying the port height with the change in engine speed to improve the delivery ratio characteristics of crankcase-scavenged two-stroke cycle engines.

ACKNOWLEDGMENTS

The authors wish to thank T. Toyoda at Toyota Automobile Corp. who assisted with much of the experimental and construction work, M. Tone, K. Yanagihara, Y. Nakatsugawa, N. Sakai, K. Sappa, T. Miyamoto, T. Koda, and K. Miyake were most closely associated with this work and their help is most sincerely appreciated.

The authors also wish to thank Dr. I. Watanabe and Dr. Benjamin L. Sheaffer for their appropriate guidance and advice.

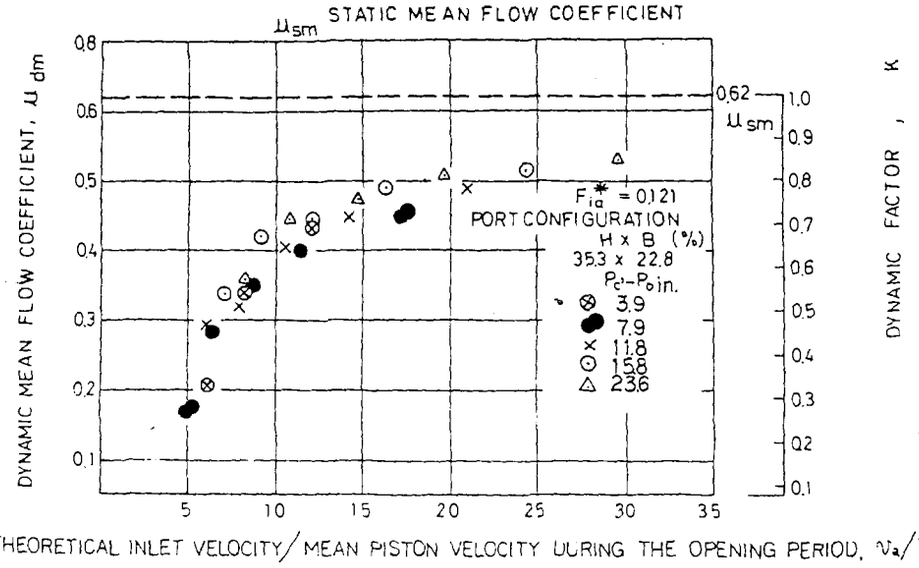

Fig. 40(c) - Relation between dynamic mean flow coefficient μdm and $V_a/\overline{V}_p$

REFERENCES, PART 2

1. E. Watanabe and K. Komotori, "Study of the Delivery Ratio Characteristics of a Crankcase-Scavenged Rotary Disk-Valve Inlet Port Two-Stroke Cycle Engine." Paper 143 presented at meeting of Japan Soc. Mech. Engrs., 1965, p. 121.

2. M. Maekawa, "On the Nozzles at Low Reynolds Numbers with a View of Measuring Pulsating Flow of Gases." Transactions, Japan Soc. Mech. Engrs., Vol. 37 (1934), No. 209, p. 599.

3. T. Sasaki, "The Coefficient of Discharge to the Scavenging and Exhaust Ports of Two-Stroke Cycle Engine." Transactions, Japan Soc. Mech. Engrs., Vol. 1 (1936), No. 2, p. 139.

4. T. Suda and T. Ishimaru, "Porting of 2 Cycle Gasoline Engines." Journals, SAE of Japan, Vol. 16 (1962), No. 4, p. 200.

5. F. Nagao, U. Shimamoto, and M. Miyake, "Effect of the Induction Pipe in a Crankcase-Scavenged Two-Cycle Engine." Japan Soc. Mech. Engrs., Vol. 26 (1961) No. 171, p. 1675. See also paper 670030, "The Effect of Crankcase Volume and the Inlet System on the Delivery Ratio of Two-Stroke Cycle Engines," presented at SAE Automotive Engineering Congress, Detroit, January 1967.

6. H. List, "Der Ladungswechsel der Verbrennungskraftmaschine." Springer Verlag, Vol. 4 (1950), No. 2, p. 16.

7. T. Saito and H. Okamura, "Study on the Flow Area of a Uniflow Two-Cycle Diesel Engine." Paper 101 presented at Meeting of Japan Soc. Mech. Engrs., 1964, p. 25.

8. L. J. Kastner, T. J. Williams, and J. B. White, "Poppet Inlet Valve Characteristics and Their Influence on the Induction Process." P.I.M.E., Vol. 178 (1963-64) No. 36, p. 955.

9. J. A. Pope, "Techniques Used in Achieving a High Specific Airflow for High-Output, Medium-Speed Diesel Engine." Transactions of the ASME, Journal of Engineering for Power, No. 4 (1967), p. 245.

10. Ref. 6, pp. 18, 38, 41, 135.

11. R. S. Benson, "Experiments on Two-Stroke Engine Exhaust Ports Under Steady and Unsteady Flow Conditions." P.I.M.E., Vol. 173, (1959), No. 19, p. 511.

12. K. Tanaka, "Air Flow through Suction Valve of Conical Seat." Rep. Aero. Res. Inst. Tokyo Imp. Univ., Nos. 17, 22, 27, 1929.

13. Ref. 6, Vol. 3 (1952), p. 47.

14. A. H. Shapiro, "The Dynamics and Thermodynamics of Compressible Fluid Flow." Vol. 1, pp. 100, 359, Ronald Press, 1953.

15. M. V. Ramamoorthy and K. Seetharamaiah, "Quadrant Edge Orifice-Modification for Better Performance." La Houille Blanche, No. 3 (1966), p. 313.

APPENDIX B - Part 2

Terms concerning ports are defined as follows:

$$Fia = \int_{\theta_{io}}^{\theta_{ic}} F_i(\theta) \cdot d\theta$$ (inlet port angle area)

$$Fsa = \int_{\theta_{so}}^{\theta_{sc}} F_s(\theta) \cdot d\theta$$ (scavenging port angle area)

$$Fea = \int_{\theta_{eo}}^{\theta_{ec}} Fe(\theta) \cdot d\theta$$ (exhaust port angle area)

$$Fr = \sqrt{\frac{F_s^2 \cdot F_e^2}{F_e^2 + F_s^2}}$$ (reduced area of the scavenging and exhaust ports)

$$Fra = \int_{\theta_{so}}^{\theta_{sc}} F_r(\theta) \cdot d\theta$$ (reduced angle area of the scavenging and exhaust ports)

$$Fia^* = \frac{\pi}{180} \cdot \frac{1}{\pi D} \cdot \frac{1}{S} \cdot Fia$$ (nondimensional inlet port angle area)

where:

F = Port area
D = Cylinder bore
S = Stroke
θ = Crank angle

Subscripts e, s, i = Exhaust, scavenging, and inlet ports, respectively.